Immune Landscape of Human Placental Villi Using Single-cell Analysis

Jessica M Toothaker[1,2], Oluwabunmi Olaloye[2], Blake T McCourt[2], Collin C McCourt[5], Tatiana N Silva[2], Rebecca M Case[5], Peng Liu[6], Dean Yimlamai[2], George Tseng[6], Liza Konnikova[1-4*]

[1]Department of Immunology, University of Pittsburgh, PA, USA
[2]Department of Pediatrics, [3]Reproductive Sciences, [4]Program in Human Translational Immunology, Yale University, New Haven, CT, USA
[5]Department of Pediatrics, Children's Hospital of Pittsburgh of UPMC, Pittsburgh, PA, USA
[6]Department of Biostatistics, University of Pittsburgh, Pittsburgh, PA, USA

*****To whom correspondence should be addressed: Liza Konnikova liza.konnikova@yale.edu

Key words: placenta, immune cells, pregnancy, T cells

Summary statement: This study used mass cytometry to identify a complex and diverse immune profile in the healthy mid-gestation human placenta at single-cell resolution.

Abstract

Maintenance of healthy pregnancy is reliant on successful balance between the fetal and maternal immune systems. Although maternal mechanisms responsible have been well studied, those used by the fetal immune system remain poorly understood. Using suspension mass cytometry and various imaging modalities, we report a complex immune system within the mid-gestation (17-23 weeks) human placental villi (PV). Consistent with recent reports in other fetal organs, T cells with memory phenotypes, though rare in abundance, were detected within the PV tissue and vasculature. Moreover, we determined T cells isolated from PV samples may be more proliferative than adult T cells at baseline after T cell receptor (TCR) stimulation. Collectively, we identified multiple subtypes of fetal immune cells within the PV and specifically highlight the enhanced proliferative capacity of fetal PV T cells.

Introduction

Successful pregnancy is dependent on balanced immune homeostasis, yet many of the factors required to maintain this homeostasis remain elusive. It is understood that the maternal immune system must balance pathogen defense while preventing rejection of the semi-allogenic fetus (Erlebacher, 2013; PrabhuDas et al., 2015). The progression of pregnancy is mirrored by distinct physiological states throughout the body requiring the maternal immunity to be dynamic and adaptive. A point illustrated by Agheepour and colleagues that tracked maternal immunological responses throughout pregnancy via mass cytometry (CyTOF) (Aghaeepour et al., 2017). Many studies have identified numerous mechanisms by which maternal immunity accommodates the fetus. These include: suppressive uterine NK cells reviewed in (Gaynor and Colucci, 2017), T regulatory (Treg) populations (Salvany-Celades et al., 2019), suppressive B cells (Huang et al., 2017), restricted access to plasmacytoid dendritic cells (pDC) (Li et al., 2018) and a predominance of type 2 helper T cells (Miyazaki et al., 2003). The importance of the maternal immune system in pregnancy cannot be understated, however recent findings suggest that the fetal immune system must also be considered.

Historically, the fetal and neonatal immune systems were thought to be immature. This hypothesis was supported by poor vaccine responses in neonates (Saso and Kampmann, 2017), high susceptibility to infection (Simonsen et al., 2014), and the predominance of naïve lymphocytes in human cord blood (Paloczi, 1999). Novel insights suggest that the fetal and neonatal immune systems are developed, though potentially have altered functions. Work supporting this includes: in utero maturation following fetal Tregs education (Mold et al., 2008), detection of novel immunosuppressive cell types present in neonates (Elahi et al., 2013; Halkias et al., 2019; Miller et al., 2018a), and the presence of in utero memory lymphocytes in many fetal tissues (Li et al., 2019; Odorizzi et al., 2018; Schreurs et al., 2019; Stras et al., 2019b; Zhang et al., 2014). However, the presence of phenotypically mature fetal leukocytes in the mid-gestation human placenta has yet to be explored.

Recent single cell RNA-sequencing studies of the first trimester fetal-maternal interface revealed previously undocumented PV cell types (Suryawanshi et al., 2018; Vento-Tormo et al., 2018). Similarly, detection of novel cell populations was observed in third trimester placental surveys (Pavličev et al., 2017; Pique-Regi et al., 2019). The work by Pique-Regi specifically identified PV-specific immune cell signatures, notably the presence of both resting and activated T cells of fetal origin in term PV (Pique-Regi et al., 2019). These data align with work detecting T cells with activated phenotypes in third trimester preterm rhesus macaques PV (Toothaker et

al., 2020). Of note, these single-cell surveys lacked histological data and as such there is a gap in knowledge as to the localization (fetal blood or PV stroma) of the immune sell types.

We hypothesized that the active PV immune system detected in the third trimester (Pique-Regi et al., 2019; Toothaker et al., 2020) is present at mid-gestation. Using RNA-sequencing, CyTOF, imaging mass cytometry (IMC), and florescent microscopy, we investigated the PV immune profile from healthy mid-gestation (17-23 weeks) placental tissues. With this unique cohort, we detected multiple PV-specific immune signatures representative of both blood and PV stromal immune cells. We also identify that PD-L1 expression on antigen presenting cells is reduced in preterm placentas highlighting the importance of regulating of PV immune cells in healthy pregnancy, Furthermore, using flow cytometry we uncovered that though rare in abundance, T cells isolated from PV samples representing T cells in both the fetal blood and PV stroma are hyperproliferative compared to adult T cells from both matched maternal decidua and unrelated adult intestines.

Results

The human mid-gestation PV have tissue specific immune signatures

We collected placental specimens from 19 second trimester products of conception, gestational age (GA) 17-23 weeks **(Table S1)**. Maternal decidua and fetal chorionic/amniotic membranes covering the chorionic plate (referred to hereafter as CP) were separated from the PV **(Fig 1A)** with forceps under a dissecting microscope. Separation of layers was initially confirmed by histology **(Fig 1B)**. Tissue was then either cryopreserved for CyTOF analysis, as previously described (Konnikova et al., 2018; Stras et al., 2019b) and validated in **Fig S1A**, fixed with formalin prior to embedding in paraffin for imaging mass cytometry (IMC) and immunofluorescence (IF) analysis or snap frozen for bulk RNA-sequencing (RNAseq). To verify separation of placental layers, we used bulk RNAseq from 3 matched cases (**Table S1**). Differential expression analysis (**Table S2**) and hierarchical clustering confirmed segregation of layers based on transcription profiles with the exception of one outlier (CP3) sample which was enriched for inflammatory signatures, likely upregulated during the D&E procedure or secondary to undocumented in utero inflammation **(Fig 1C)**. Segregation of samples was further confirmed with k-means clustering which grouped samples correctly by tissue with the exception of CP3 outlier **(Fig 1C)**. Moreover, we confirmed the enrichment of decidua and PV specific stromal

genes previously identified (Pique-Regi et al., 2019; Suryawanshi et al., 2018; Vento-Tormo et al., 2018). To determine if immune cells in the mid-gestation PV were solely reflective of the classical Hofbauer cell population we used immunofluorescence to co-stain for CD45, a marker of all hematopoietic cells and CD163, a classical PV resident Hofbauer cell marker (Reyes and Golos, 2018). Consistent with previous reports identifying non-Hofbauer immune subsets in the second (Bonney et al., 2000), first, and third (Pique-Regi et al., 2019) trimester PV, we detected $CD45^{pos}CD163^{lo}$ cells within the mid-gestation PV **(Fig 1D)** ranging in abundance from 30-70% of $CD45^{pos}$ nuclei per high power field **(Fig S1B)**. As the PV are bathed in maternal blood (intervillous), we also confirmed that immune cells present in PV samples were reflective of cells contained within the trophoblast layers PV itself (intravillous) and not contaminate maternal cells **(Fig 1D, S1B)**. Additionally, we detected the Y chromosome with *in situ* hybridization in many intravillous cells and had enriched expression of Y chromosome derived *EIF1AY* mRNA and low expression of the X chromosome inactivation transcript *XIST* in male PV samples indicating that the majority PV immune cells were fetal **(Fig 1E, S1C)**. We next assessed immune gene expression via RNAseq. Though most transcripts in the PV were expressed lower than decidual counterparts (darker in color), transcripts for a large number of immune subtypes analyzed were detected in PV samples (circle size) **(Fig 1F, Table S3)**.

To survey the $CD45^{pos}$ populations in the PV, we used 38 metal conjugated antibodies **(Table S4)** and performed CyTOF analysis on 12 placenta-matched decidua, CP and PV samples **(Table S1)**. Briefly, cryopreserved tissues were batch thawed and digested to make single cell suspensions, stained with antibodies and analyzed using CyTOF (Konnikova et al., 2018) **(Fig S1A)**. FCS files from CyTOF analysis were pre-gated for DNA^{pos}, single, live, non-bead, $CD45^{pos}$ cells **(Fig S2A)**. After omitting samples with insufficient cell numbers (>750 $CD45^{pos}$ cells) we were left with 11 samples for each tissue **(Table S5)**. $CD45^{pos}$ cells were clustered using Phenograph **(Fig 2A)** and identified based on surface markers from Clustergrammer generated associated heatmaps **(Table S6, Fig S2B)**.

To confirm that PV immune subsets identified were not solely reflective of blood leukocytes in the fetal circulation, we used immunofluorescence (IF) and imaging mass cytometry (IMC) with a panel that included 23 markers **(Table S8)** on 6 total regions of 2 individual PV cases **(Table S1)**. Using IMC, we validated that B cells, DCs, T cells and Mϕs were outside the fetal vasculature (CD31) in the PV stroma **(Fig 2B-F)**. To identify NK cells and ILCs, we used dual *in situ* hybridization and immunofluorescence **(Fig 2C, G)**. Though it is likely that some PV immune cells detected with CyTOF represent blood leukocytes, we conclude that a proportion of the PV immune cells are stromal.

To further characterize these cells, we used CyTOF analysis consisting of 31 unique clusters of immune cells within the STP, belonging to Mϕ, DC, NK, CD4 T cell, CD8 T cell, double positive (DP) T cell, B cell and other immune cell type subsets **(Fig 2H, S2B)**. Overall, immune cell subsets were in the minority in abundance of all live cells found in the placenta **(Fig S2C)**. However, each layer of the placenta still housed a unique and complex immune profile **(Fig S2D)**. When all clusters belonging to the same immune subset were combined, the decidua had a greater abundance of NK cells compared to PV **(Fig 2H),** consistent with previous studies (King et al., 1991; Koopman et al., 2003). Additionally, there was a higher proportion of CD4 T cells in the decidua than either of the fetal layers **(Fig 2H)**. In contrast, the PV had a larger proportion of Mϕ (potentially Hofbauer cells) **(Fig 2H)**.

When each cluster abundance was directly compared, 11/31 $CD45^{pos}$ clusters were differently distributed between the three layers of the placenta **(Fig 2I-J, S2E)**. The PV was uniquely enriched for cluster 19 $CCR7^{neg}$ Mϕs **(Fig 1I-J).** This robust cluster similarly suggests the presence of Hofbauer cells (as prior reports show most Hofbauer cells are $CCR7^{neg}$ (Joerink et al., 2011)) in the PV and confirms the tissue-specificity of Hofbauer cells in our data set due to this cluster being largely undetectable in decidua and CP samples **(Fig 2J)**. Interestingly, we also found cluster 10, $CCR7^{neg}$ DCs, and cluster 3, $CD69^{neg}$ CD8 T cells, to be enriched in the PV over decidua **(Fig 2I-J)**. CCR7 is highly expressed on DCs homing to secondary lymphoid structures from peripheral tissues after antigen encounter (Ohl et al., 2004). CD69 is found to be transiently upregulated on activated T cells (Cibrián and Sánchez-Madrid, 2017) and constitutively upregulated on tissue resident memory T cells (Kumar et al., 2017). As PV enriched clusters 9 and 3 lacked these respective markers, we hypothesize that PV are poised to execute mature immune function, such as antigen presentation, but may not actively performing such functions in utero. To further explore this idea, we next analyzed each immune cell subset more thoroughly.

PV innate cells have quiescent phenotypes

To evaluate PV non-antigen presenting innate cells that represent the first cells to sense foreign antigens, we clustered on $CD3^{neg}CD19^{neg}HLA\text{-}DR^{neg}$ cells (**Fig S3A)**. We identified Mϕs, innate lymphoid cells (ILCs), NK cells and multiple other immune cell populations that we were unable to fully phenotype with our panel **(Table S4), (Fig 3A, S3B)**. When comparing subtypes of immune cells, we confirmed our findings from the CD45 level (**Fig 2A)**, with the decidua

having a larger proportion of NK cells and the PV having a larger proportion of Mϕs **(Fig 2H)**. The increased granularity of focusing on HLA-DR^{neg} innate cells, revealed that the PV contains CD163^{hi} Mϕs likely Hofbauer cells, and contained a significant proportion CD163^{lo} Mϕs, presumably other non-classical Hofbauer cell Mϕs; Hofbauer cells that had down regulated CD163 expression; or fetal blood monocytes **(Fig 3B)**. HLA-DR^{neg} Mϕs in the decidua, in contrast were largely CD163^{hi}, consistent with previous data on the phenotype of decidual Mϕs (Jiang and Wang, 2020) and with the enriched CD163 gene signatures seen in the decidua over CP from RNAseq data **(Fig 1F).** The Mϕ profile in the CP was more equally split between the two CD163^{lo} phenotypes **(Fig 3B)**. At the individual cluster level, multiple clusters were enriched in either the decidua and/or CP **(Fig S3C)**. PV were enriched in cluster 25, CD163^{lo} Mϕs, and cluster 27, NK cells **(Fig 3C)**. While cluster 27 NK cells were abundant in all three placental layers and only slightly elevated in the PV, cluster 25 Mϕs were specific to the PV and were only minimally present in decidua and CP **(Fig 3C)**.

To determine if PV NK and ILCs were expressing activation markers, we compared the mean metal intensities (MMIs) of CD69 and PD-1 on these cells and found that PV NK cells and ILCs expressed significantly lower amounts of both CD69 and PD-1 **(Fig 3D)**. Next, to examine if PV innate cells have migratory or tissue-retentive phenotypes we compared chemokine receptor (CCR) expression among subsets. Illustrated both visually **(Fig 3E)** and graphically **(Fig 3F)** we show that multiple populations of PV innate cells including NK cells, ILC and CD163^{hi} Mϕs had reduced expression of four CCRs. Interestingly, the expression of these markers between the three compartments was similar for the CD163^{lo} Mϕs (**Fig 3F**). To determine if other chemokine receptor/ligand pairs were also reduced in the PV, we identified 19 chemokine receptors/ligands that were differentially expressed between PV, CP and decidua using bulk RNA-seq **(Fig 3G, Table S7)**. These results validated the CyTOF findings of reduced expression of CCR6 and CXCR3 specifically, as well as at least one ligand for CCR7 and CCR4. Nine other chemokine ligand/receptors were implicated in this dataset **(Fig 3G).**

PV antigen presenting cells are diverse and phenotypically immunosuppressive

Next, we examined APC populations within each placental layer by clustering on CD45^{pos} CD3^{neg} HLA-DR^{pos} cells **(Fig S4A)**. We identified seven sub-types of APCs including: myeloid DCs (mDCs), plasmacytoid DCs (pDCs), CD163^{hi} Mϕs, CD163^{lo} Mϕs, B cells, NK cells and other cell types that we could not identify based on the available markers **(Fig 4A, S4B)**. In confirmation of our previous findings **(Fig 2-3)**, NK cells were again more prevalent in the

decidua compared to the PV **(Fig 4B)**. HLA-DR^{pos} NK cells that are capable to independently present antigens to CD4 T cells have been described (Roncarolo et al., 1991). In contrast to HLA-DR^{neg} innate cells **(Fig 3)**, numerous individual APC clusters were enriched in the PV **(Fig 4C)**. Of note, multiple populations were enriched in the decidua and CP as well **(Fig S4C)**. Specifically, B cell clusters 7 and 27, mDC clusters 16 and 20, and CD163^{lo} CD4^{neg} Mϕ clusters 6 and 22 were significantly more abundant in the PV than either decidua or CP **(Fig 4C)**. Complimenting this finding, CD4^{pos}CD163^{hi} Mϕs (cluster 26) were reduced in the PV compared to decidua and CP **(Fig S4C).** CD4^{pos} Mϕs have been shown to be long lived tissue resident Mϕs in the intestine and perhaps they serve a similar role in the decidua (Shaw et al., 2018). The large number of APC clusters (11 in total) differentially abundant between the PV and decidua/CP suggests that antigen presentation in the PV may be functioning through non-classical mechanisms at mid-gestation.

To investigate phenotypes unique to PV APCs, we examined the expression of both activation and immunosuppressive markers on each APC subset identified in **Figure 4B**. In contrast to the hypothesis that PV APCs have altered ability to function as APCs compared to decidua and CP, we found no difference in HLA-DR expression among APC subsets **(Fig 4D)**. However, consistent with the hypothesis of PV APCs being more inhibited than decidua and CP counterparts, we identified significantly reduced expression of the activation maker CD69 in the PV CD163^{hi} Mϕs, NK cells, pDCs and mDCs **(Fig 4E)**. Furthermore, when we examined the inhibitory ligand, PD-L1, we documented its increased expression on multiple APC subsets, significantly so on CD163^{lo} Mϕs and HLA-DR^{pos} NK cells **(Fig 4F)**. This observation of high PD-L1 expression on PV APCs was confirmed by IF staining, where almost every observable PV HLA-DR^{pos} cell co-expressed PD-L1 **(Fig 4G, S4D)**.

To further explore the PD-L1 and HLA-DR signature, we labeled both PD-L1 and HLA-DR in the PV stroma with immunohistochemistry (IHC) between healthy mid-gestation placentas (21-23 weeks' gestation), preterm placentas from complicated pregnancies (29-35 weeks' gestation) and healthy placentas delivered at full-term (39 weeks' gestation) **(Fig 4H)**. Consistent with our CyTOF findings, mid-gestation stromal cells have high expression of PD-L1 per nuclei and PD-L1 staining patterns were congruent with stromal HLA-DR staining indicating that the PD-L1^{pos} cells analyzed were likely APCs **(Fig 4H)**. Of note, we discovered that stromal PD-L1 expression in preterm PV is significantly lower than that of mid-gestation and term PV. Furthermore, term PV also had significantly reduced PD-L1 expression on stromal cells than mid-gestation PV **(Fig 4H)**. In contrast, we observed increased PD-L1 expression on preterm trophoblasts compared to mid-gestation trophoblasts **(Fig S4E)**. To confirm that the reduction of

stromal PD-L1 was not an artifact of reduced APC abundance in preterm and term placentas we compared mean HLA-DR expression between all three groups and found no differences **(Fig 4H)**. These results suggest that PD-L1 expression on PV APCs may be important for maintaining healthy pregnancy.

To investigate the regulation of constitutive PD-L1 expression we measured the expression of IFNγ, a well-documented regulator of PD-L1 (Garcia-Diaz et al., 2017). We found preferential transcription of IFNγ over TNFα at baseline by PV immune cells **(Fig 4I, S4F).** Additionally, PV immune cells transcribed comparable IFNγ, but transcribe decreased TNFα than decidual immune cells **(Fig S4G)**. The preferential production of IFNγ to TNFα was confirmed in PV immune cells with flow cytometry. We report that IFNγ was mostly derived from non-NK innate immune cells **(Fig 4J)**. As such, it is possible that PV immune cells produce IFNγ to drive expression of PD-L1 on APCs.

The second trimester placenta is dominated by memory CD8 T cells

As we observed high PD-L1 expression on APCs, we next explored if there were T cells present in the PV that could potentially be inhibited by immunosuppressive APCs. We identified both circulating (within blood vessel) and potentially tissue resident T cells in the PV **(Fig 5A, S5A)**. Moreover, using IMC, we surprisingly identified non-circulating T cells of CD4, CD8 and double negative (DN) phenotypes that expressed CD45RO, a marker upregulated after antigen experience and absent on naïve T cells **(Fig 5B, S5B)**. Turning to our CyTOF data, when clustering specifically on T cells **(Fig S5C)**, we found that all three layers of the placenta had a T cell profiles dominated by CD8 T Cells **(Fig 5C-D, S5D)**. Building off the initial detection of CD45RO by IMC, we found that the majority of T cells in the PV were of memory phenotypes, delineated based on lack of expression of CCR7 and CD45RA **(Fig 5E)**. Additionally, we found CD8 T cells with tissue-resident memory (TRM) phenotype in all three layers **(Fig 5E)**. We detected $CD69^{pos}$ T cells both as a marker of TRMs on $CCR7^{neg}$ $CD45RA^{neg}$ T cells and also among other T cell subsets **(Fig 5E)**. The expression of CD69 on multiple T cell populations strongly suggests that some populations of PV T cells are stromal and not reflective of fetal blood T cells, because recent work has shown that blood CD8 T cells do not express CD69 (Buggert et al., 2020). The detection of both $CD69^{neg}$ and $CD69^{pos}$ CD8 T cells in the PV is consistent with the enrichment of one cluster of $CD69^{neg}$ CD8 T cells from our initial $CD45^{pos}$ clustering **(Fig 2)**. CD8 and CD4 non-Treg cell subtypes were evenly distributed between all three layers **(Fig 5D)**. However, CD4 Tregs were enriched in the decidua compared to the PV

(Fig 5D). The abundance and importance of Tregs throughout pregnancy in the decidua is well documented (Mjösberg et al., 2010; Salvany-Celades et al., 2019), but the role of Tregs in the CP and the PV is unclear, though we have shown PV Tregs function abnormally during intraamniotic inflammation (Toothaker et al., 2020). Moreover, there was an enrichment of $CD4^{neg}$ $CD8^{neg}$ that were also $CD56^{neg}$ double negative (DN) T cells in the PV **(Fig 5D, S5D)**. These DN T cells could potentially be $\gamma\delta$ T cells whose presence in the first trimester PV has been described (Bonney et al., 2000).

The detection of PV T cells expressing memory markers in human mid-gestation PV is novel. To investigate T cell signatures unique to the PV, we next compared the abundance of individual T cell clusters. While two clusters were enriched in the decidua **(Fig S5E)**, cluster 9 $CD4^{neg}$ $CD8^{neg}$ T cells, cluster 4 CM CD8 T cells, and cluster 11 CD4 T cells were enriched in the PV **(Fig 5F)**. Cluster 11 T cells were $CCR4^{pos}CXCR3^{neg}CCR6^{neg}$ **(Fig 5F, S5D)**, surface marker expression pattern suggestive of a TH2 phenotype, however further analysis for detection of TH2 specific transcription factors (GATA3) is needed for confirmation.

Resting phenotypes define PV T cell subsets

We next explored if a resting phenotype was consistent among PV T cell subsets identified in **Fig 5D**. Among non-TRM T cells, PV T cell subsets exhibit reduced expression of CD69 **(Fig 5G, S5F)**. Moreover, the PV housed fewer $PD\text{-}1^{pos}$ cells **(Fig 5H)** and reduced PD-1 per T cell compared to decidual counterparts **(Fig 5I-J)**. Though PD-1 is a marker of T cell exhaustion, it is also upregulated upon activation of the TCR (summarized in (Xu-Monette et al., 2017)). We propose this is the more likely role of observed down-regulation of PD-1 in PV T cells as it is consistent with the downregulation of CD69.

PV T cell activation potential

To determine if PV T cells have a reduced activation profile, we scanned for activated T cells via HLA-DR, phosphorylated Histone H3, phosphorylated S6 and phosphorylated CREB in T cells using IMC. We identified both resting **(Fig 6A)** and activated T cells in the PV **(Fig 6B)**. We next questioned if mid-gestation PV T cells could be activated in a TCR dependent manner. To test the functionality of the TCR pathway in PV T cells, we stimulated single cell suspensions from PV with soluble αCD3 and αCD28 antibodies for 4 hours. We observed an increase in abundance of rapidly proliferating T cells by high Ki67 expression (Miller et al., 2018b) in fetal T

cells (placenta and intestine) compared to adult T cells (decidua and intestine) **(Fig 6C, S6B)**, validating our previous findings that PV T cells are fetal in origin and unique from the decidua. Of note, the placenta had the highest proportion of rapidly proliferating cells across all organs and ages following stimulation **(Fig 6C)**.

In summary **(Fig 7)**, we demonstrate that the intravillous compartment of the healthy second trimester PV contains a diverse immune landscape comprised of innate cells such as Mϕs, NK cells and ILCs, as well as APCs including B cells, and memory T cells **(Fig 2)**. Moreover, we show that the immune cells in the PV maintain decreased levels of activation markers at baseline as a potential mechanism for preventing in utero inflammation. The mechanisms described include reducing chemotaxis by reduced expression of chemokine receptors on innate cells and low transcription of chemokine ligands in the PV overall **(Fig 3)**. Moreover, PV APCs constitutively express PD-L1, possibly regulated by the high expression of IFNγ by PV immune cells **(Fig 4)**. Finally, phenotypically mature PV T cells **(Fig 5)** proliferate upon activation through the TCR pathway **(Fig 6)**.

Discussion

Preserving tolerance at the fetal-maternal interface is critical for maintaining a healthy pregnancy. How leukocytes within the PV contribute to immune homeostasis has yet to be fully elucidated. Single cell studies of first trimester (Suryawanshi et al., 2018; Vento-Tormo et al., 2018) and full term (Pavličev et al., 2017; Pique-Regi et al., 2019) placenta highlighted the diversity of immune cells within the PV. We hypothesized that the activated leukocytes detected in humans (Pique-Regi et al., 2019) and non-human primates (Toothaker et al., 2020) may be present in the PV earlier in gestation. We analyzed placental tissue and confirmed that there are diverse immune cells of fetal origin in second trimester PV samples within the intravillous space. Although it is possible that our analysis of PV immune cells included a proportion of maternal cells, ethical limitations precluded maternal peripheral blood collection. Future studies are needed to determine the exact origin of individual immune cell populations as either fetal blood immune cells within the PV vasculature and PV-resident cells in the stroma.

Previous studies suggest that PV fetal immune cells are limited to Hofbauer cells (Thomas et al., 2021). The increased granularity provided by single cell methods allowed for the detection of T cells, B cells and NK cells in healthy term placentas (Pique-Regi et al., 2019). Moreover, a recent study identified infiltrating cells in the PV to be largely of fetal origin in

infectious villitis (Enninga et al., 2020) and Erbach et *al.* isolated T cells from single cell suspension at 18-24 weeks' gestation (Erbach et al., 1993). It is important to note that studies using cell suspensions make the delineation of immune cells from the PV vasculature indistinguishable from those in the stroma. By combining CyTOF and multiple imaging modalities, we identified both innate and adaptive immune cells, present outside the fetal vasculature in the intravillous space.

Thomas et *al.* reported that Hofbauer cells in the first trimester are HLA-DR^{neg} (Thomas et al., 2021), consistent with this we found an increased abundance of Mϕs in the PV compared to the decidua. Surprisingly, we report that many of these HLA-DR^{neg} Mϕs in the PV had reduced expression of CD163, a marker reported to be expressed in all Hofbauer cells (Reyes and Golos, 2018; Schliefsteiner et al., 2017). It is possible that CD163^{lo} Mϕs reflect downregulation of CD163 by Hofbauer cells during cell isolation (Tang et al., 2011). It is also possible that Hofbauer cells are more diverse than previously thought and CD163 should be used in combination with other Mϕ markers in future studies.

We identified phenotypes consistent with an anti-inflammatory state for multiple subsets of PV immune cells. We found that innate non-APCs expressed lower levels of multiple chemokine receptors than decidual counterparts consistent with histologic evaluation of Hofbauer cells showing a lack of CCR7 staining (Joerink et al., 2011). This coupled with reduced expression of multiple chemokine pathways could suggest that innate cells in the PV are either static or are mobile in a non-targeted manner at baseline. We also identified HLA-DR^{pos} cells including mDCs, pDCs, B cells, Mϕs and a population of HLA-DR^{pos} NK cells. An antigen-presenting role for NK cells has been previously described (Roncarolo et al., 1991). The identification of fetal HLA-DR^{pos} Mϕs contrasts Thomas et ***al's*** recent findings (Thomas et al., 2021). It should be noted that some of these HLA-DR^{pos} Mϕs in our study may reflect contaminate maternal Mϕs repairing breaks in the trophoblast layer. However, the location of HLA-DR^{pos} cells by both immunofluorescent and IMC show that some cells are located distant from the trophoblast layer and suggest that HLA-DR^{pos} Mϕs appear in the stroma after the time period studied by Thomas et al. It would be interesting to determine the fetal versus maternal origin of these HLA-DR^{pos} Mϕs and evaluate if the Hofbauer cell population from 18-23 weeks is transcriptionally distinct from those in prior studies (Vento-Tormo et al., 2018).

Irrespective of PV APC ontogeny, we determined that PV APCs express more PD-L1 per cell than decidual counterparts. PD-L1's function as a coinhibitory molecule has been extensively studied (Sun et al., 2018). Moreover, PD-L1 expression can be mediated through interferon (IFNγ) (Garcia-Diaz et al., 2017). We found PV immune cells produce IFNγ preferentially to TNFα. In further validation, we found that preterm PV have significantly reduced expression of PD-L1 on PV stromal cells compared to mid-gestation PV. Though it is not possible to determine if PD-L1 reduction precedes or is the consequence of preterm delivery.

Detection of memory T cells within the PV justifies the need for PV APCs to limit T cell activation. Memory T cells have been detected in multiple fetal human organs (Angelo et al., 2019; Halkias et al., 2019; Li et al., 2019; Schreurs et al., 2019; Stras et al., 2019a), and within the non-human primate PV (Toothaker et al., 2020). Additionally activated and resting T cells have been detected in PV samples post-delivery (Pique-Regi et al., 2019) and central memory T cell can be found in human cord blood (Frascoli et al., 2018). We found PV T cells express low activation signatures potentially suggesting that PV T cells have been previously educated but remain quiescent due to either the lack of antigens or direct inhibition from APCs.

The presence of a fetal microbiome as a source of antigens remains highly contested (Aagaard et al., 2014; de Goffau et al., 2019; Kuperman et al., 2020; Leiby et al., 2018; Mishra et al., 2021; Rackaityte et al., 2020; Theis et al., 2020). Our group recently showed that bacterial metabolites are present in the fetal intestine at 14 weeks' gestation (Li et al., 2020). As such, it is possible that maternal bacteria derived peptides similarly cross the placenta and educate fetal T cells. Fetal T cell activation by maternal antigens has also been implicated in preterm birth (Frascoli et al., 2018). Our data indicates that PV T cells can be stimulated through the activation of the TCR signaling (αCD3/CD28 antibodies). Collectively, these findings have identified the unique hyper-proliferative potential of PV T cells compared to adult T cells and fetal intestinal T cells and suggest that antigens could stimulate a PV T cell response in utero.

Our study had several limitations of note the lack of genetic information to segregate fetal from maternal cells. It would be very interesting for a future cohort to definitively determine the origin of each PV immune cell subset identified in this work using dual *in situ* hybridization and immunodetection techniques. Legal limitations prevented the collection of maternal and fetal blood to use for comparison.

The ability of fetal immune cells to execute mature functions has recently been validated in multiple fetal organs (Angelo et al., 2019; Frascoli et al., 2018; Halkias et al., 2019; McGovern et al., 2017; Schreurs et al., 2019; Stras et al., 2019b). The detection of immunosuppressive mechanisms to control this fetal immune response and prevent in utero inflammation is critical.

We have identified previously understudied immune cell populations within the mid-gestation PV. This work has implications for future studies to better understand the roles of fetal and maternal immune cells within the placenta and contribute to a better understanding of immune tolerance in multiple diseases.

Methods

Placental Tissue Collection

Human products of conception were obtained through the University of Pittsburgh Biospecimen core after IRB approval (IRB# PRO18010491). Tissue was collected only from subjects that signed an informed consent to allow use for research purposes. Preterm placentas resultant from a variety of obstetric complications were obtained from the University of Pittsburgh MOMI Biobank. Term placentas were collected both at the University of Pittsburgh through the MOMI biobank and through the Yale University YURS Biobank from C-section deliveries devoid of obstetric complications (**Table S1**). The n values for each experiment are illustrated as a checklist in Table S1. Placental villi were separated using forceps under a light dissection microscope (Fisherbrand #420430PHF10) from the chorionic and amniotic membranes lining the chorionic plate (CP) and from the decidua basilis (referred to as decidua throughout manuscript) on the basal plate side of the placenta. Tissue was thoroughly washed with sterile PBS prior to cryopreservation and subsequent single cell isolation as previously described (Konnikova et al., 2018).

RNA sequencing: Snap frozen placental tissues were shipped on dry ice to MedGenome for mRNA extraction and library preparation. RNA extractions were completed with the Qiagen All Prep Kit (#80204). cDNA synthesis was prepped with the Takara SMART-seq kit (#634894) and NexteraXT (FC-131-1024, Illumina) was used to fragment and add sequencing adaptors. Quality control was completed by MedGenome via Qubit Fluorometric Quantitation and TapeStation BioAnalyzer. Libraries were sequenced on the NovaSeq6000 for Paired End 150 base pairs for 90 million reads per sample.

RNA sequencing analysis: FASTQ files were imported and subsequently analyzed with CLC Genomics Workbench 20.0 (https://digitalinsights.qiagen.com). Briefly, paired reads were first trimmed with a quality limit of 0.05, ambiguous limit of 2 with automated read through adapter trimming from the 3'-end with a maximum length of 150. Trimmed reads were then mapped to the homo_sapiens_sequence_hg38 reference sequence. Differential gene expression was computed in CLC Genomics with an Across groups ANOVA-like comparison. Significantly differentially expressed genes were delineated as those with a p-value <0.05, False-Discovery Rate <20% and fold-change > absolute value of 2. Heatmaps for gene expression were created with Morpheus (https://software.broadinstitute.org/morpheus).

RISH: Formalin fixed samples were sectioned and embedded in paraffin by the Pitt Biospecimen Core. Staining was completed per manufacturer's instructions for RNAScope® multiplex V2 detection kit (ACD Bio) coupled with immunofluorescent protein staining for either Cytokeratin19 (ab52625, Abcam) at 1:250 dilution. Echo® Revolve microscope at 20x was used to image sections. All images were batch processed using FIJI (Schindelin et al., 2012), and all edits were made to every pixel in an image identically across all patients per experiment. Quantification of cell populations was done using a custom pipeline in CellProfiler (McQuin et al., 2018).

FISH*:* In situ hybridization for the Y chromosome was adapted from the protocol outlined in (Enninga et al., 2020). Briefly, slides were deparaffinized with a series of xylene and ethanol washes. Target retrieval was done at 95^{oC} for 10 minutes, slides were placed in 70% ethanol, 85% ethanol and 100% ethanol for 2 minutes each. DYZ3 probe (D5J10-034, Abbott Laboratories) was diluted 1:10 in LSI/WCP hybridization buffer (D6J67-011, Abbott Laboratories) and incubated for 5 minutes at 83^{oC} prior to overnight hybridization at 37^{oC}. Slides were soaked in SSC/0.1% NP-40 (ab142227, Abcam) to remove cover slips and placed in 2X SSC/0.1% NP-40 for 2 minutes at 74^{oC} before mounting with antifade plus Propidium Iodide (p36935, Invitrogen). Slides were imaged on the LSM 710 (Leica Biosystems) confocal at the Yale Center for Cellular and Molecular Imaging.

RNA extraction and qPCR: RNA was extracted from snap-frozen villi samples using the RNAEasy Minikit (#217004, Qiagen) RNA was converted to cDNA using iScript (#1708891, BioRad) reagents according to manufacturer protocol. Samples were run on the Taqman StepOnePlus Real-Time PCR System (Applied Biosciences) machine with probes for ACTB

(Hs01060665_g1) as housekeeping gene and with either XIST (Hs01079824_m1) or EIF3AY (Hs01040047) all from Qiagen. Values undeterminable were given cycle values of 40 for quantification purposes.

Immunofluorescent staining: Slides with 10um sections of FFPE tissue were deparaffinized with a series of xylene and ethanol washes. Antigen retrieval was performed in the Biocare Medical LLC decloaking chamber (NC0436641) for 1 hour with citrate-based antigen retrieval buffer (H-3300, Vector Laboratories) and washed with PBS. Slides were then blocked for 30 minutes with 10% horse serum prior to overnight incubation at 4^{o}C with primary antibodies in 2% horse serum. Primary antibodies used were Cytokeratin19 (ab192751, Abcam) at 1:1000 dilution; CD45 (20103-1-AP, Proteintech) at 1:200 dilution; CD163 (ab87099, Abcam) at 1:200 dilution; CD3 (ab135372, Abcam) at 1:100 dilution; CD31 (ab9498, Abcam) at 1:1000 dilution. Slides were washed with PBS and incubated with Alexa Fluor secondary antibodies (donkey anti-rabbit IgG H&L 555, ab150074; donkey anti-mouse IgG H&L 647, ab150107; goat anti-guinea pig IgG H&L 488, ab150185) 2% horse serum at 1:750 dilution for 45 minutes at RT. Slides were mounted with Antifade mounting media + DAPI (H-1300, Vectashield).

Imaging mass cytometry: Slides with 4um sections of FFPE tissue were deparaffinized with a series of xylene and ethanol washes. Antigen retrieval was performed at 95^{oC} for 20 minutes using 1X Antigen Retrieval Buffer (#CTS013 R&D) and washed with water and dPBS. Slides were then blocked for 30 minutes with 3% BSA in dPBS prior to overnight incubation at 4^{o}C with a primary antibody cocktail **(Table S8)**. Slides were rinsed and co-stained with 191/193 DNA-intercalator (Fluidigm), rinsed and air dried for >20 minutes prior to analysis. Slides were analyzed on the Hyperion Mass Cytometer with an ablation energy of 4 and frequency of 100Hz for ~30 minutes per section. Representative images were generated using Histocat++ software (Catena et al., 2018).

CyTOF staining*:* Samples were stained with antibody cocktail (**Table S4**) per previously published protocol (Stras et al., 2019b) and incubated with 191Ir/193Ir DNA intercalator (Fluidigm) and shipped overnight to the Longwood Medical Area CyTOF Core. Data was normalized and exported as FCS files, downloaded and uploaded to Premium Cytobank® platform. Any files with insufficient cell number were excluded from analysis **(Table S5)**. Gating and analysis was completed with cytofkit (Chen et al., 2016) as published (Stras et al., 2019b). Cluster abundance was extracted, and statistically analyzed using R.

Stimulation of PV T cells: Cells were isolated from cryopreserved PV samples as described throughout manuscript. Dead cells were removed prior to stimulation using Millitenyl dead cell removal kit (130-090-101 Millitenyl Biotec). Cells were incubated with αCD3 (clone HIT3a, #300302, Biolegend) and αCD28 (clone CD28.2, 302902, Biolegend) soluble antibodies for 4 hours rotating at 37^{oC} + 5% CO_2 in the presence of GolgiPlug (51-2301K2, BD Biosciences) GolgiStop (51-2092K2, BD Biosciences).

Flow cytometry*:* Post stimulation cells were washed with PBS and incubated with Zombie Aqua live/dead stain. Viability marker was washed out and cells were resuspended and spun down in FACS buffer then incubated with Human TruStain FcX (Biolegend) for 10 minutes prior to the addition or a surface antibody cocktail **(Table S9)** Cells were washed with FACs buffer and permeabilized with FoxP3 fix/perm (Invitrogen) overnight. Cells were washed with 1X FoxP3 Wash Buffer (Invitrogen) and incubated with intracellular antibodies. Cells were washed, fixed for 10 minutes with 4% PFA and resuspended in FACs buffer. All samples were run on All samples were run on BD LSRII (BDBiosciences) at the Yale University Flow Cytometry core (all other stimulations). Output FCS files were analyzed with FlowJo®.

Statistics*:* R version 3.6.1 with Kruskal-Wallis analysis and Dunn's multiple comparison test for post-hoc analysis among groups. One-tailed t-test was used to compare groups of two. Comparisons of mean expression values corrected using the Bonferroni method. P-values of 0.05 or less were significant.

Plot generation: Plots comparing multiple groups were generated using Prism GraphPad 8. In each plot, each data point represents one subject as per figure description.

Data and code availability: Data analyzed in this study has been stored according to IRB guidelines and is subject to institutional regulations. Requests can be directed to Lead Contact, Liza Konnikova liza.konnikova@yale.edu. Bulk mRNA extracted from three issues isolated from matched placentas was deposited at (https://www.ncbi.nlm.nih.gov/geo/). The GEO accession number is GSE178152.

Acknowledgements: This project used the UPMC Hillman Cancer Center and Tissue and Research Pathology/Pitt Biospecimen Core shared resource which is supported in part by award P30CA047904. This research was supported in part by the University of Pittsburgh

Center for Research Computing through the resources provided. We thank Yale Flow Cytometry for their assistance with LSRII service. The Core is supported in part by an NCI Cancer Center Support Grant # NIH P30 CA016359. We also thank Ansen Burr and the Hand Lab at The University of Pittsburgh for their help with RNA-sequencing analysis and Meghan Mooring and Dean Yimlamai for help with confocal microscopy and Biorender images.

Funding: JMT was supported by 5T32AI089453-10 and the University of Pittsburgh. LK is supported by previous startup funds from University of Pittsburgh and current start-up funds from Yale University, Binational Science Foundation award number 2019075, and National Institute of Health R21TR002639 and R21HD102565. No NIH funds were used for the fetal work of these studies.

Author Contributions: JMT and LK conceived the work**.** CyTOF and flow cytometry procedures and analysis and drafting of manuscript were done by JMT supervised by LK. Tissue collection and preparation was done by JMT, RMC, CCM and OOO. IMC analysis was done by OOO. Immunocytochemistry was completed by BTM; RISH was done by RMC; RNA extraction/qPCR was performed by CCM. Cytometry bioinformatics consultation was done with PL supervised by GT. RNA sequencing assistance provided by DY. Figure construction was done by JMT, TNS, BTM. All authors contributed to the editing and compilation of the manuscript.

Declaration of Interests: The authors have declared that no conflict of interest exists.

References

Aagaard, K., Ma, J., Antony, K. M., Ganu, R., Petrosino, J. and Versalovic, J. (2014). The placenta harbors a unique microbiome. *Sci. Transl. Med.* **6**, 237ra65.

Aghaeepour, N., Ganio, E. A., Mcilwain, D., Tsai, A. S., Tingle, M., Van Gassen, S., Gaudilliere, D. K., Baca, Q., McNeil, L., Okada, R., et al. (2017). An immune clock of human pregnancy. *Sci. Immunol.* **2**,.

Angelo, L. S., Bimler, L. H., Nikzad, R., Aviles-Padilla, K. and Paust, S. (2019). CXCR6+ NK cells in human fetal liver and spleen possess unique phenotypic and functional capabilities. *Front. Immunol.* **10**, 469.

Bonney, E. A., Pudney, J., Anderson, D. J. and Hill, J. A. (2000). Gamma-delta T cells in midgestation human placental villi. *Gynecol Obstet Invest* **50**, 153–157.

Buggert, M., Vella, L. A., Nguyen, S., Wu, V. H., Chen, Z., Sekine, T., Perez-Potti, A., Maldini, C. R., Manne, S., Darko, S., et al. (2020). The Identity of Human Tissue-Emigrant CD8+ T Cells. *Cell* **183**, 1946–1961.e15.

Catena, R., Montuenga, L. M. and Bodenmiller, B. (2018). Ruthenium counterstaining for imaging mass cytometry. *J. Pathol.* **244**, 479–484.

Chen, H., Lau, M. C., Wong, M. T., Newell, E. W., Poidinger, M. and Chen, J. (2016). Cytofkit: A bioconductor package for an integrated mass cytometry data analysis pipeline. *PLoS Comput. Biol.* **12**, e1005112.

Cibrián, D. and Sánchez-Madrid, F. (2017). CD69: from activation marker to metabolic gatekeeper. *Eur. J. Immunol.* **47**, 946–953.

de Goffau, M. C., Lager, S., Sovio, U., Gaccioli, F., Cook, E., Peacock, S. J., Parkhill, J., Charnock-Jones, D. S. and Smith, G. C. S. (2019). Human placenta has no microbiome but can contain potential pathogens. *Nature* **572**, 329–334.

Elahi, S., Ertelt, J. M., Kinder, J. M., Jiang, T. T., Zhang, X., Xin, L., Chaturvedi, V., Strong, B. S., Qualls, J. E., Steinbrecher, K. A., et al. (2013). Immunosuppressive CD71+ erythroid cells compromise neonatal host defence against infection. *Nature* **504**, 158–162.

Enninga, E. A. L., Raber, P., Quinton, R. A., Ruano, R., Ikumi, N., Gray, C. M., Johnson, E. L., Chakraborty, R. and Kerr, S. E. (2020). Maternal T Cells in the Human Placental Villi Support an Allograft Response during Noninfectious Villitis. *J. Immunol.* **204**, 2931–2939.

Erbach, G. T., Semple, J. P., Milford, E., Goguen, J., Osathanondh, R. and Kurnick, J. T. (1993). Phenotypic characteristics of lymphocyte populations isolated from middle gestation human placenta. *J Reprod Immunol* **25**, 1–13.

Erlebacher, A. (2013). Immunology of the maternal-fetal interface. *Annu. Rev. Immunol.* **31**, 387–411.

Frascoli, M., Coniglio, L., Witt, R., Jeanty, C., Fleck-Derderian, S., Myers, D. E., Lee, T.-H., Keating, S., Busch, M. P., Norris, P. J., et al. (2018). Alloreactive fetal T cells promote uterine contractility in preterm labor via IFN-γ and TNF-α. *Sci. Transl. Med.* **10**,.

Garcia-Diaz, A., Shin, D. S., Moreno, B. H., Saco, J., Escuin-Ordinas, H., Rodriguez, G. A., Zaretsky, J. M., Sun, L., Hugo, W., Wang, X., et al. (2017). Interferon Receptor Signaling Pathways Regulating PD-L1 and PD-L2 Expression. *Cell Rep.* **19**, 1189–1201.

Gaynor, L. M. and Colucci, F. (2017). Uterine natural killer cells: functional distinctions and influence on pregnancy in humans and mice. *Front. Immunol.* **8**, 467.

Halkias, J., Rackaityte, E., Hillman, S. L., Aran, D., Mendoza, V. F., Marshall, L. R., MacKenzie, T. C. and Burt, T. D. (2019). CD161 contributes to prenatal immune suppression of IFNγ-producing PLZF+ T cells. *J. Clin. Invest.* **129**, 3562–3577.

Huang, B., Faucette, A. N., Pawlitz, M. D., Pei, B., Goyert, J. W., Zhou, J. Z., El-Hage, N. G., Deng, J., Lin, J., Yao, F., et al. (2017). Interleukin-33-induced expression of PIBF1 by decidual B cells protects against preterm labor. *Nat. Med.* **23**, 128–135.

Jiang, X. and Wang, H. (2020). Macrophage subsets at the maternal-fetal interface. *Cell Mol Immunol* **17**, 889–891.

Joerink, M., Rindsjö, E., van Riel, B., Alm, J. and Papadogiannakis, N. (2011). Placental macrophage (Hofbauer cell) polarization is independent of maternal allergen-sensitization and presence of chorioamnionitis. *Placenta* **32**, 380–385.

Kim, J. S., Romero, R., Kim, M. R., Kim, Y. M., Friel, L., Espinoza, J. and Kim, C. J. (2008). Involvement of Hofbauer cells and maternal T cells in villitis of unknown aetiology. *Histopathology* **52**, 457–464.

King, A., Balendran, N., Wooding, P., Carter, N. P. and Loke, Y. W. (1991). $CD3^-$ Leukocytes Present in the Human Uterus During Early Placentation: Phenotypic and Morphologic Characterization of the $CD56^{++}$ Population. *Dev. Immunol.* **1**, 169–190.

Konnikova, L., Boschetti, G., Rahman, A., Mitsialis, V., Lord, J., Richmond, C., Tomov, V. T., Gordon, W., Jelinsky, S., Canavan, J., et al. (2018). High-dimensional immune phenotyping and transcriptional analyses reveal robust recovery of viable human immune and epithelial cells from frozen gastrointestinal tissue. *Mucosal Immunol.* **11**, 1684–1693.

Koopman, L. A., Kopcow, H. D., Rybalov, B., Boyson, J. E., Orange, J. S., Schatz, F., Masch, R., Lockwood, C. J., Schachter, A. D., Park, P. J., et al. (2003). Human decidual natural killer cells are a unique NK cell subset with immunomodulatory potential. *J. Exp. Med.* **198**, 1201–1212.

Kumar, B. V., Ma, W., Miron, M., Granot, T., Guyer, R. S., Carpenter, D. J., Senda, T., Sun, X., Ho, S.-H., Lerner, H., et al. (2017). Human Tissue-Resident Memory T Cells Are Defined by Core Transcriptional and Functional Signatures in Lymphoid and Mucosal Sites. *Cell Rep.* **20**, 2921–2934.

Kuperman, A. A., Zimmerman, A., Hamadia, S., Ziv, O., Gurevich, V., Fichtman, B., Gavert, N., Straussman, R., Rechnitzer, H., Barzilay, M., et al. (2020). Deep microbial analysis of multiple placentas shows no evidence for a placental microbiome. *BJOG* **127**, 159–169.

Leiby, J. S., McCormick, K., Sherrill-Mix, S., Clarke, E. L., Kessler, L. R., Taylor, L. J., Hofstaedter, C. E., Roche, A. M., Mattei, L. M., Bittinger, K., et al. (2018). Lack of detection of a human placenta microbiome in samples from preterm and term deliveries. *Microbiome* **6**, 196.

Li, Y., Lopez, G. E., Vazquez, J., Sun, Y., Chavarria, M., Lindner, P. N., Fredrickson, S., Karst, N. and Stanic, A. K. (2018). Decidual-Placental Immune Landscape During Syngeneic Murine Pregnancy. *Front. Immunol.* **9**, 2087.

Li, N., van Unen, V., Abdelaal, T., Guo, N., Kasatskaya, S. A., Ladell, K., McLaren, J. E., Egorov, E. S., Izraelson, M., Chuva de Sousa Lopes, S. M., et al. (2019). Memory CD4+ T cells are generated in the human fetal intestine. *Nat. Immunol.* **20**, 301–312.

Li, Y., Toothaker, J. M., Ben-Simon, S., Ozeri, L., Schweitzer, R., McCourt, B. T., McCourt, C. C., Werner, L., Snapper, S. B., Shouval, D. S., et al. (2020). In utero human intestine harbors unique metabolome, including bacterial metabolites. *JCI Insight*.

McGovern, N., Shin, A., Low, G., Low, D., Duan, K., Yao, L. J., Msallam, R., Low, I., Shadan, N. B., Sumatoh, H. R., et al. (2017). Human fetal dendritic cells promote prenatal T-cell immune suppression through arginase-2. *Nature* **546**, 662–666.

McQuin, C., Goodman, A., Chernyshev, V., Kamentsky, L., Cimini, B. A., Karhohs, K. W., Doan, M., Ding, L., Rafelski, S. M., Thirstrup, D., et al. (2018). CellProfiler 3.0: Next-generation image processing for biology. *PLoS Biol.* **16**, e2005970.

Miller, D., Romero, R., Unkel, R., Xu, Y., Vadillo-Ortega, F., Hassan, S. S. and Gomez-Lopez, N. (2018a). CD71+ erythroid cells from neonates born to women with preterm labor regulate cytokine and cellular responses. *J. Leukoc. Biol.* **103**, 761–775.

Miller, I., Min, M., Yang, C., Tian, C., Gookin, S., Carter, D. and Spencer, S. L. (2018b). Ki67 is a Graded Rather than a Binary Marker of Proliferation versus Quiescence. *Cell Rep.* **24**, 1105–1112.e5.

Mishra, A., Lai, G. C., Yao, L. J., Aung, T. T., Shental, N., Rotter-Maskowitz, A., Shepherdson, E., Singh, G. S. N., Pai, R., Shanti, A., et al. (2021). Microbial exposure during early human development primes fetal immune cells. *Cell*.

Miyazaki, S., Tsuda, H., Sakai, M., Hori, S., Sasaki, Y., Futatani, T., Miyawaki, T. and Saito, S. (2003). Predominance of Th2-promoting dendritic cells in early human pregnancy decidua. *J. Leukoc. Biol.* **74**, 514–522.

Mjösberg, J., Berg, G., Jenmalm, M. C. and Ernerudh, J. (2010). FOXP3+ regulatory T cells and T helper 1, T helper 2, and T helper 17 cells in human early pregnancy decidua. *Biol. Reprod.* **82**, 698–705.

Mold, J. E., Michaëlsson, J., Burt, T. D., Muench, M. O., Beckerman, K. P., Busch, M. P., Lee, T.-H., Nixon, D. F. and McCune, J. M. (2008). Maternal alloantigens promote the development of tolerogenic fetal regulatory T cells in utero. *Science* **322**, 1562–1565.

Odorizzi, P. M., Jagannathan, P., McIntyre, T. I., Budker, R., Prahl, M., Auma, A., Burt, T. D., Nankya, F., Nalubega, M., Sikyomu, E., et al. (2018). In utero priming of highly functional effector T cell responses to human malaria. *Sci. Transl. Med.* **10**,.

Ohl, L., Mohaupt, M., Czeloth, N., Hintzen, G., Kiafard, Z., Zwirner, J., Blankenstein, T., Henning, G. and Förster, R. (2004). CCR7 governs skin dendritic cell migration under inflammatory and steady-state conditions. *Immunity* **21**, 279–288.

Paloczi, K. (1999). Immunophenotypic and functional characterization of human umbilical cord blood mononuclear cells. *Leukemia* **13 Suppl 1**, S87-9.

Pavličev, M., Wagner, G. P., Chavan, A. R., Owens, K., Maziarz, J., Dunn-Fletcher, C., Kallapur, S. G., Muglia, L. and Jones, H. (2017). Single-cell transcriptomics of the human placenta: inferring the cell communication network of the maternal-fetal interface. *Genome Res.* **27**, 349–361.

Pique-Regi, R., Romero, R., Tarca, A. L., Sendler, E. D., Xu, Y., Garcia-Flores, V., Leng, Y., Luca, F., Hassan, S. S. and Gomez-Lopez, N. (2019). Single cell transcriptional signatures of the human placenta in term and preterm parturition. *Elife* **8**,.

PrabhuDas, M., Bonney, E., Caron, K., Dey, S., Erlebacher, A., Fazleabas, A., Fisher, S., Golos, T., Matzuk, M., McCune, J. M., et al. (2015). Immune mechanisms at the maternal-fetal interface: perspectives and challenges. *Nat. Immunol.* **16**, 328–334.

Rackaityte, E., Halkias, J., Fukui, E. M., Mendoza, V. F., Hayzelden, C., Crawford, E. D., Fujimura, K. E., Burt, T. D. and Lynch, S. V. (2020). Viable bacterial colonization is highly limited in the human intestine in utero. *Nat. Med.* **26**, 599–607.

Reyes, L. and Golos, T. G. (2018). Hofbauer cells: their role in healthy and complicated pregnancy. *Front. Immunol.* **9**, 2628.

Romero, R., Espinoza, J., Gonçalves, L. F., Kusanovic, J. P., Friel, L. A. and Nien, J. K. (2006). Inflammation in preterm and term labour and delivery. *Semin Fetal Neonatal Med* **11**, 317–326.

Roncarolo, M. G., Bigler, M., Haanen, J. B., Yssel, H., Bacchetta, R., de Vries, J. E. and Spits, H. (1991). Natural killer cell clones can efficiently process and present protein antigens. *J. Immunol.* **147**, 781–787.

Salvany-Celades, M., van der Zwan, A., Benner, M., Setrajcic-Dragos, V., Bougleux Gomes, H. A., Iyer, V., Norwitz, E. R., Strominger, J. L. and Tilburgs, T. (2019). Three Types of Functional Regulatory T Cells Control T Cell Responses at the Human Maternal-Fetal Interface. *Cell Rep.* **27**, 2537–2547.e5.

Saso, A. and Kampmann, B. (2017). Vaccine responses in newborns. *Semin Immunopathol* **39**, 627–642.

Schindelin, J., Arganda-Carreras, I., Frise, E., Kaynig, V., Longair, M., Pietzsch, T., Preibisch, S., Rueden, C., Saalfeld, S., Schmid, B., et al. (2012). Fiji: an open-source platform for biological-image analysis. *Nat. Methods* **9**, 676–682.

Schliefsteiner, C., Peinhaupt, M., Kopp, S., Lögl, J., Lang-Olip, I., Hiden, U., Heinemann, A., Desoye, G. and Wadsack, C. (2017). Human Placental Hofbauer Cells Maintain an Anti-inflammatory M2 Phenotype despite the Presence of Gestational Diabetes Mellitus. *Front. Immunol.* **8**, 888.

Schreurs, R. R. C. E., Baumdick, M. E., Sagebiel, A. F., Kaufmann, M., Mokry, M., Klarenbeek, P. L., Schaltenberg, N., Steinert, F. L., van Rijn, J. M., Drewniak, A., et al. (2019). Human Fetal TNF-α-Cytokine-Producing CD4+ Effector Memory T Cells Promote Intestinal Development and Mediate Inflammation Early in Life. *Immunity* **50**, 462–476.e8.

Shaw, T. N., Houston, S. A., Wemyss, K., Bridgeman, H. M., Barbera, T. A., Zangerle-Murray, T., Strangward, P., Ridley, A. J. L., Wang, P., Tamoutounour, S., et al. (2018). Tissue-resident macrophages in the intestine are long lived and defined by Tim-4 and CD4 expression. *J. Exp. Med.* **215**, 1507–1518.

Simonsen, K. A., Anderson-Berry, A. L., Delair, S. F. and Davies, H. D. (2014). Early-onset neonatal sepsis. *Clin. Microbiol. Rev.* **27**, 21–47.

Stras, S. F., Warner, L., Toothaker, J. M., Olaloye, O. O., Oldham, A. L., McCourt, C. C., Lee, Y. N., Rechavi, E., Shouval, D. S. and Konnikova, L. (2019a). Maturation of the Human Intestinal Immune System Occures Early During Fetal Development. *Dev. Cell*.

Stras, S. F., Werner, L., Toothaker, J. M., Olaloye, O. O., Oldham, A. L., McCourt, C. C., Lee, Y. N., Rechavi, E., Shouval, D. S. and Konnikova, L. (2019b). Maturation of the human intestinal immune system occurs early in fetal development. *Dev. Cell* **51**, 357–373.e5.

Sun, C., Mezzadra, R. and Schumacher, T. N. (2018). Regulation and Function of the PD-L1 Checkpoint. *Immunity* **48**, 434–452.

Suryawanshi, H., Morozov, P., Straus, A., Sahasrabudhe, N., Max, K. E. A., Garzia, A., Kustagi, M., Tuschl, T. and Williams, Z. (2018). A single-cell survey of the human first-trimester placenta and decidua. *Sci. Adv.* **4**, eaau4788.

Tagliani, E. and Erlebacher, A. (2011). Dendritic cell function at the maternal-fetal interface. *Expert Rev Clin Immunol* **7**, 593–602.

Tang, Z., Tadesse, S., Norwitz, E., Mor, G., Abrahams, V. M. and Guller, S. (2011). Isolation of hofbauer cells from human term placentas with high yield and purity. *Am J Reprod Immunol* **66**, 336–348.

Theis, K. R., Romero, R., Greenberg, J. M., Winters, A. D., Garcia-Flores, V., Motomura, K., Ahmad, M. M., Galaz, J., Arenas-Hernandez, M. and Gomez-Lopez, N. (2020). No consistent evidence for microbiota in murine placental and fetal tissues. *mSphere* **5**,.

Thomas, J. R., Appios, A., Zhao, X., Dutkiewicz, R., Donde, M., Lee, C. Y. C., Naidu, P., Lee, C., Cerveira, J., Liu, B., et al. (2021). Phenotypic and functional characterization of first-trimester human placental macrophages, Hofbauer cells. *J. Exp. Med.* **218**,.

Toothaker, J. M., Presicce, P., Cappelletti, M., Stras, S. F., McCourt, C. C., Chougnet, C. A., Kallapur, S. G. and Konnikova, L. (2020). Immune Cells in the Placental Villi Contribute to Intra-amniotic Inflammation. *Front. Immunol.* **11**, 866.

Vento-Tormo, R., Efremova, M., Botting, R. A., Turco, M. Y., Vento-Tormo, M., Meyer, K. B., Park, J.-E., Stephenson, E., Polański, K., Goncalves, A., et al. (2018). Single-cell reconstruction of the early maternal-fetal interface in humans. *Nature* **563**, 347–353.

Xu-Monette, Z. Y., Zhang, M., Li, J. and Young, K. H. (2017). PD-1/PD-L1 Blockade: Have We Found the Key to Unleash the Antitumor Immune Response? *Front. Immunol.* **8**, 1597.

Yang, S. W., Cho, E. H., Choi, S. Y., Lee, Y. K., Park, J. H., Kim, M. K., Park, J. Y., Choi, H. J., Lee, J. I., Ko, H. M., et al. (2017). DC-SIGN expression in Hofbauer cells may play an important role in immune tolerance in fetal chorionic villi during the development of preeclampsia. *J Reprod Immunol* **124**, 30–37.

Zhang, X., Mozeleski, B., Lemoine, S., Dériaud, E., Lim, A., Zhivaki, D., Azria, E., Le Ray, C., Roguet, G., Launay, O., et al. (2014). CD4 T cells with effector memory phenotype and function develop in the sterile environment of the fetus. *Sci. Transl. Med.* **6**, 238ra72.

Figures

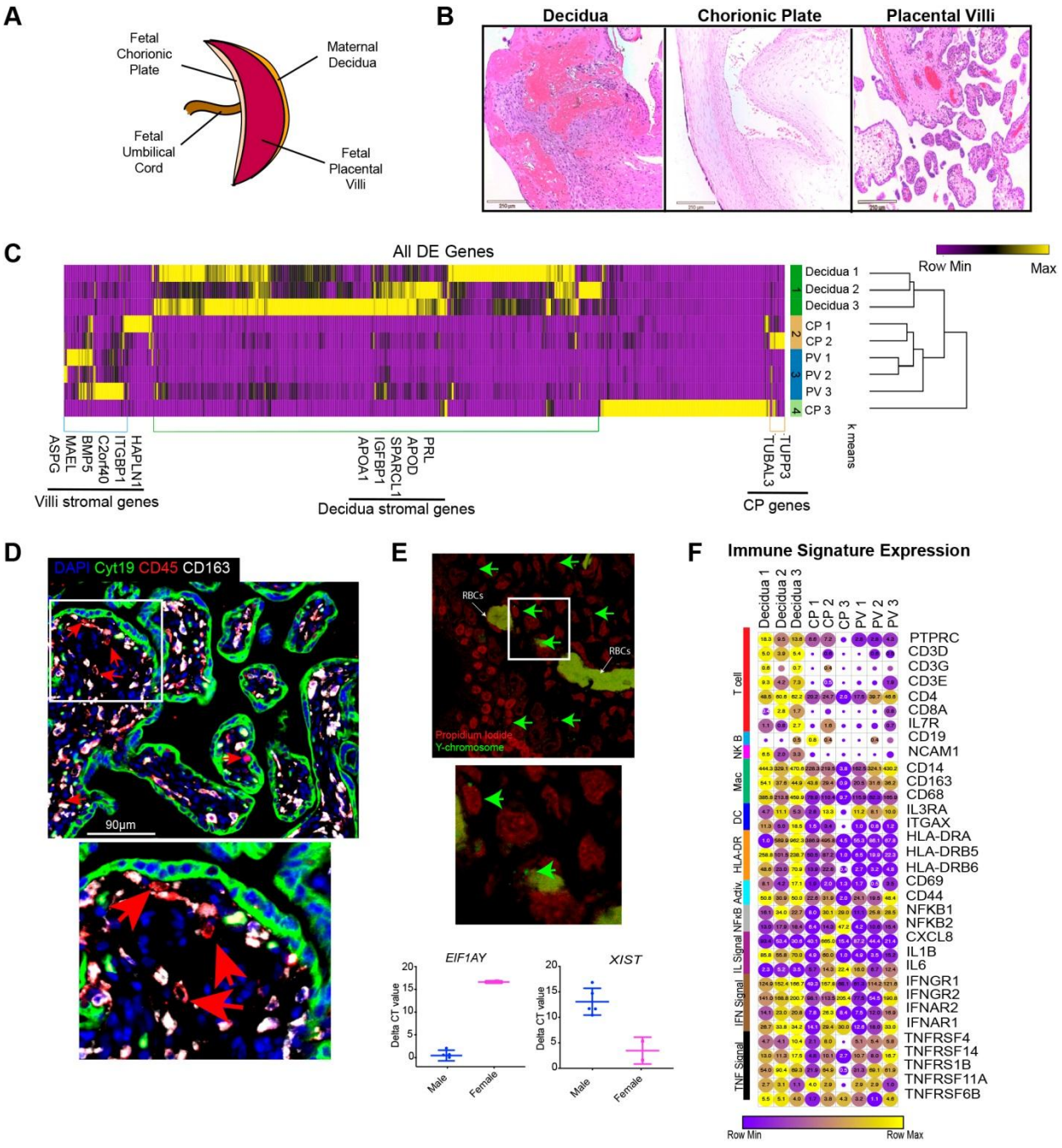

Figure 1. Tissue specific signatures in the mid-gestation placenta. (A) Diagram of placental tissues. (B) H&E staining of placental tissues (n=19). (C) All differentially expressed genes between t placental tissues with p value <0.05, false-discovery rate <20%, and fold change >absolute value 2 (n=3). (D) CD45pos CD163lo/neg cells within the intravillous space identified

with immunofluorescence (n=19). (E) Fluorescent in situ hybridization of Y chromosome in PV (top). Delta CT values of Y and X chromosome genes in male and female PV (bottom) (n=1 male, 1 female). (F) Expression values of selected immune genes. Circle size indicative of expression value. Circle color indicative of relative expression across row. (n=3 per tissue type). * = p value <0.05 upon post hoc analysis after Kruskal-Wallis (K-W) test. DE = differentially expressed. CP= chorionic plate. All graphs use mean for average values and standard error for error bars.

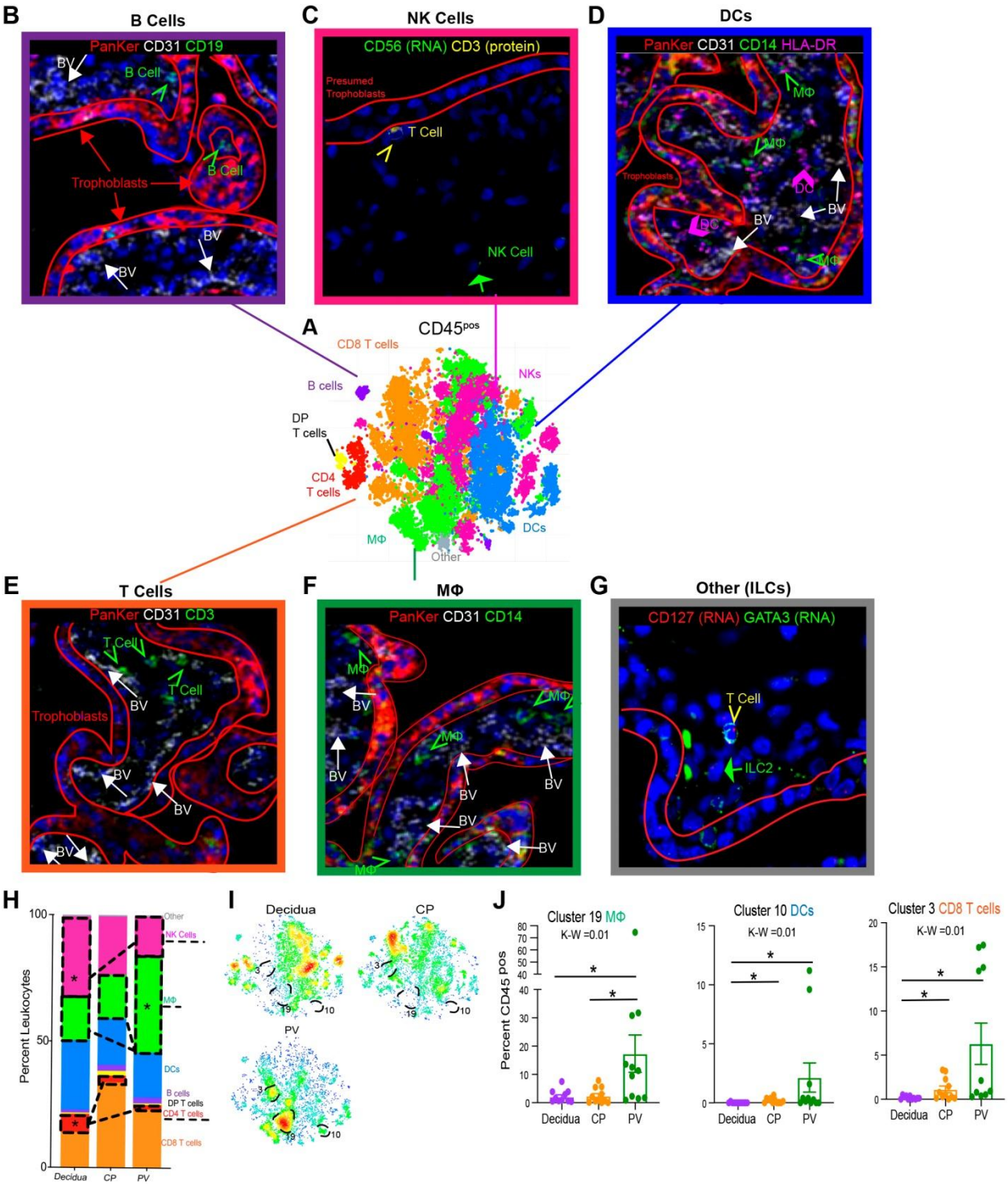

Figure 2. Global Immune Landscape of Second Trimester Placenta. (A) Merged tsne of CD45pos cells from maternal decidua (n=11), CP (n=11) and PV (n=11) from Phenograph clustering of CyTOF data. (B) IMC identifying B cells (green) arrows located within the trophoblast bound (red) and outside the fetal blood vessels (BV) (white arrows). PanKer =

pankeratin, stains for trophoblasts. (C) Dual in situ hybridization and immunofluorescence (IF) identifying NK cells (green arrow) distinct from T cell (yellow arrowhead) in PV. (D) IMC identifying DCs (pink arrows) and HLA-DRpos Mfs (green arrows). (E) IMC identifying T cells (green arrows). (F) IMC identifying Mfs (green arrows). (G) Dual in situ hybridization and IF identifying ILC2s (green arrow) distinct from T cell (yellow arrowhead) in PV. (H) Stacked bar graph comparing summation of all clusters belonging to same immune subsets from CyTOF data. (I) Density plot rof populations in (A) segregated by tissue of origin. Clusters significantly enriched in PV outlined. (J) Quantification of PV enriched cluster abundance. K-W = Kruskal-wallis test. * = p value <0.05 following posthoc analysis. All graphs use mean for average values and standard error for error bars.

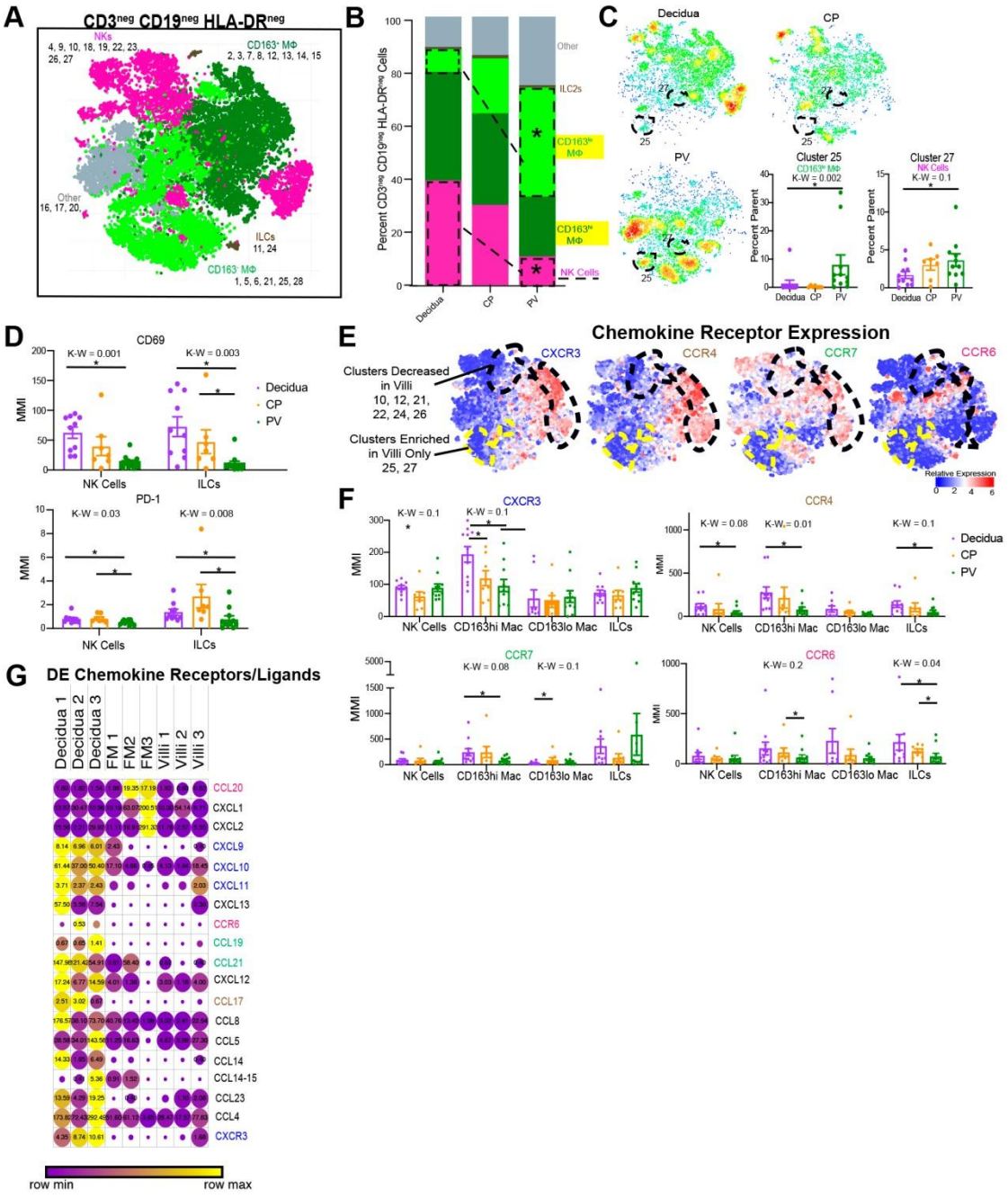

Figure 3. Innate HLA-DR^{neg} cells in PV. (A) Combined CyTOF tsne for CD45^{pos} CD3^{neg} CD19^{neg} HLA-DR^{neg} cells (n=12). (B) Stacked bar graph of abundance of major immune subtype. (C) Density plots separated by tissue of cell populations from (A). Statistically significantly abundant clusters in PV outlined. (right side) Cumulative data of PV abundant clusters outlined in density plots. (D) Mean metal intensities (MMI) of CD69 (top) and PD-1 (bottom) for 2D gated NK and ILC populations. (E) Expression heatmaps for chemokine receptors mapped to cells identified in (A). (F) MMIs of chemokine receptors on innate cell

subsets from 2D gating. (G) Expression from RNA-sequencing of differentially expressed chemokine ligand/receptor genes between tissues (n=3). Circle size indicative of expression value, circle color reflective of relative expression across row. Differentially expressed determined as: p value <0.05, false-discovery rate <20%, and fold change > absolute value 2. * = p value <0.05 upon post hoc analysis after Kruskal-Wallis (K-W) test. DE= differentially expressed. All graphs use mean for average values and standard error for error bars.

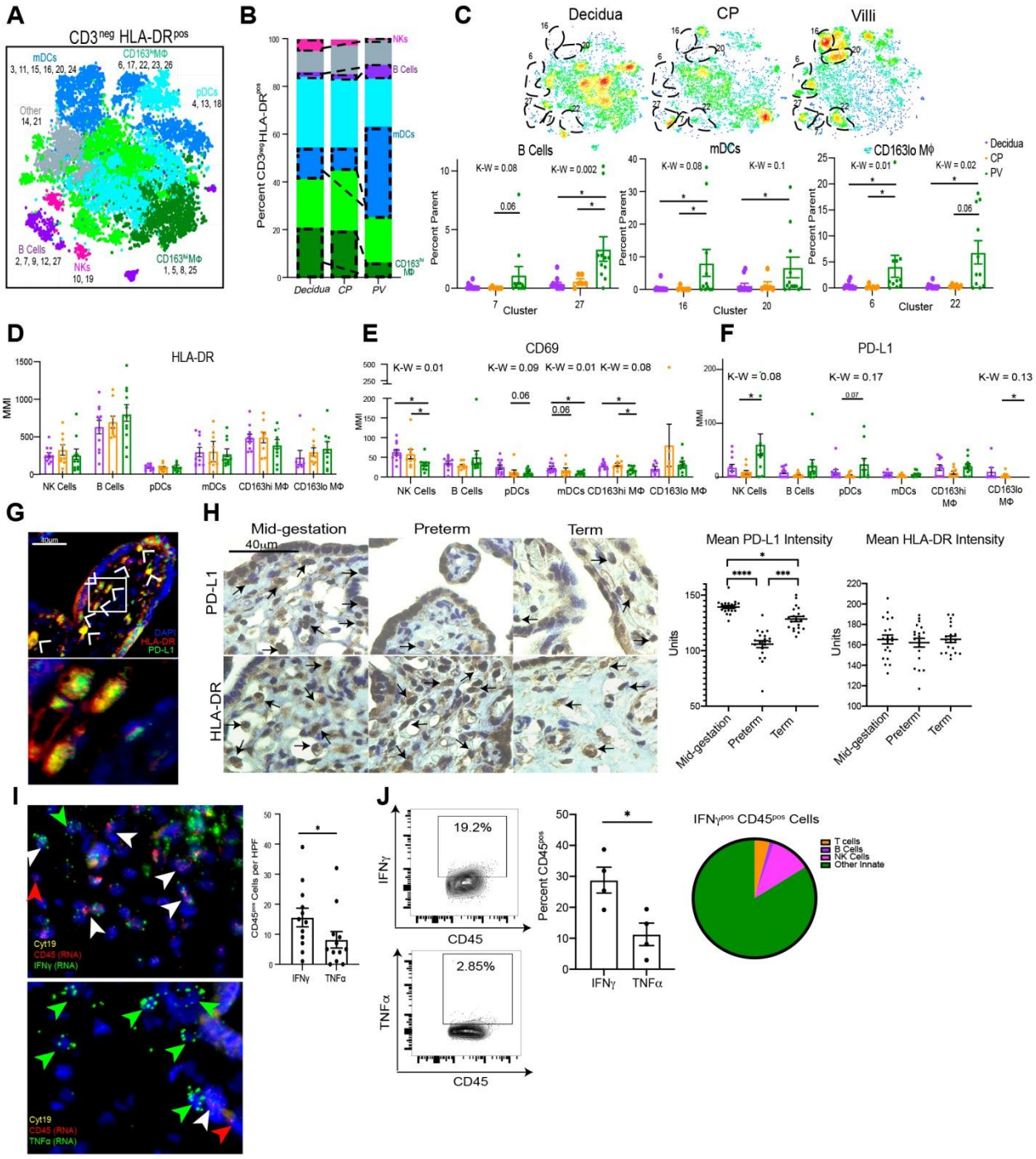

Figure 4. Antigen Presenting Cells in the PV. (A) Cumulative CyTOF tsne for CD45^{pos} CD3^{neg} HLA-DR^{pos} cells. (B) Stacked bar graph of abundance of major immune subtype. (C) Density plot separated by tissue of origin from (A). Statistically significantly abundant clusters in PV outlined. Cumulative data of PV abundant clusters outlined in density plots. MMI of HLA-DR (D), CD69 (E) and PD-L1 (F) for 2D gated populations. * = p value <0.05

upon post hoc analysis after Kruskal-Wallis test. (G) PD-L1^{pos} APC populations in PV. (H) Representative images (left) and quantification of average stain intensity per stromal nuclei (right) for PD-L1 and HLA-DR IHC. (n=2) (I) Representative images (left) and quantification of automated image analysis with CellProfiler (right) for dual RNA *in situ* hybridization and immunofluorescence in PV (n=12). (J) Flow plots and quantification for cytokine positive PV immune cells via flow cytometry. (n=4) Pie-chart of major immune subset abundance of IFNg^{pos} immune cells from flow cytometry. * = p-value <0.05 in Mann-Whitney test. K-W = Kruskal Wallis test p value. MMI = mean metal intensity. CyTOF analysis starting (n=12), see Table S5 for omitted cases. All graphs use mean for average values and standard error for error bars.

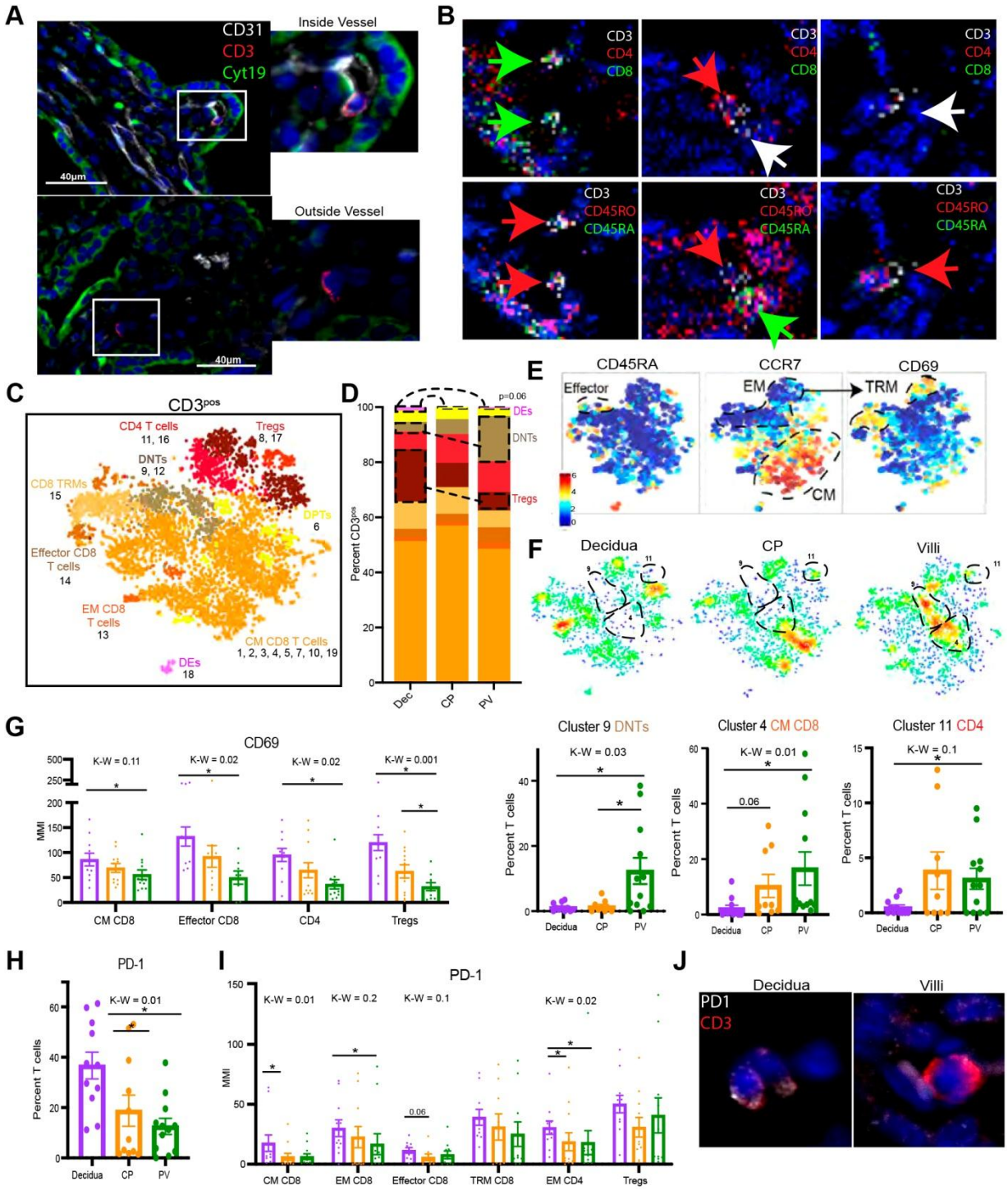

Figure 5. T cell subsets in placental tissues. Representative images of T cells inside (top) and outside (bottom) fetal vasculature (CD31) in PV. (B) IMC images of T cell subtypes in PV. (C) Cumulative CyTOF tsne for PV, CP and decidua CD45^{pos} CD3^{neg} HLA-DR^{pos} cells. (D) Stacked bar graph of abundance of major immune subtype. (E) Relative expression of memory

T cell markers in PV cell populations from (C). (F) Density plot separated by tissue of origin (C). Statistically significantly abundant clusters in PV outlined. Cumulative data of PV abundant clusters outlined in density plots. (G) MMI of CD69 from 2D gating of populations. (H) Abundance of PD-1^{pos} T cells by 2-D gating. (I) PD-1 MMI from 2D gated subsets. CyTOF analysis starting (n=12), see Table S5 for omitted cases. (J) PD-1 on T cells in PV and decidua. * = p value <0.05 upon post hoc analysis after Kruskal-Wallis (K-W) test. MMI = mean metal intensity. CM = central memory, EM = effector memory, TRM = tissue-resident memory. All graphs use mean for average values and standard error for error bars.

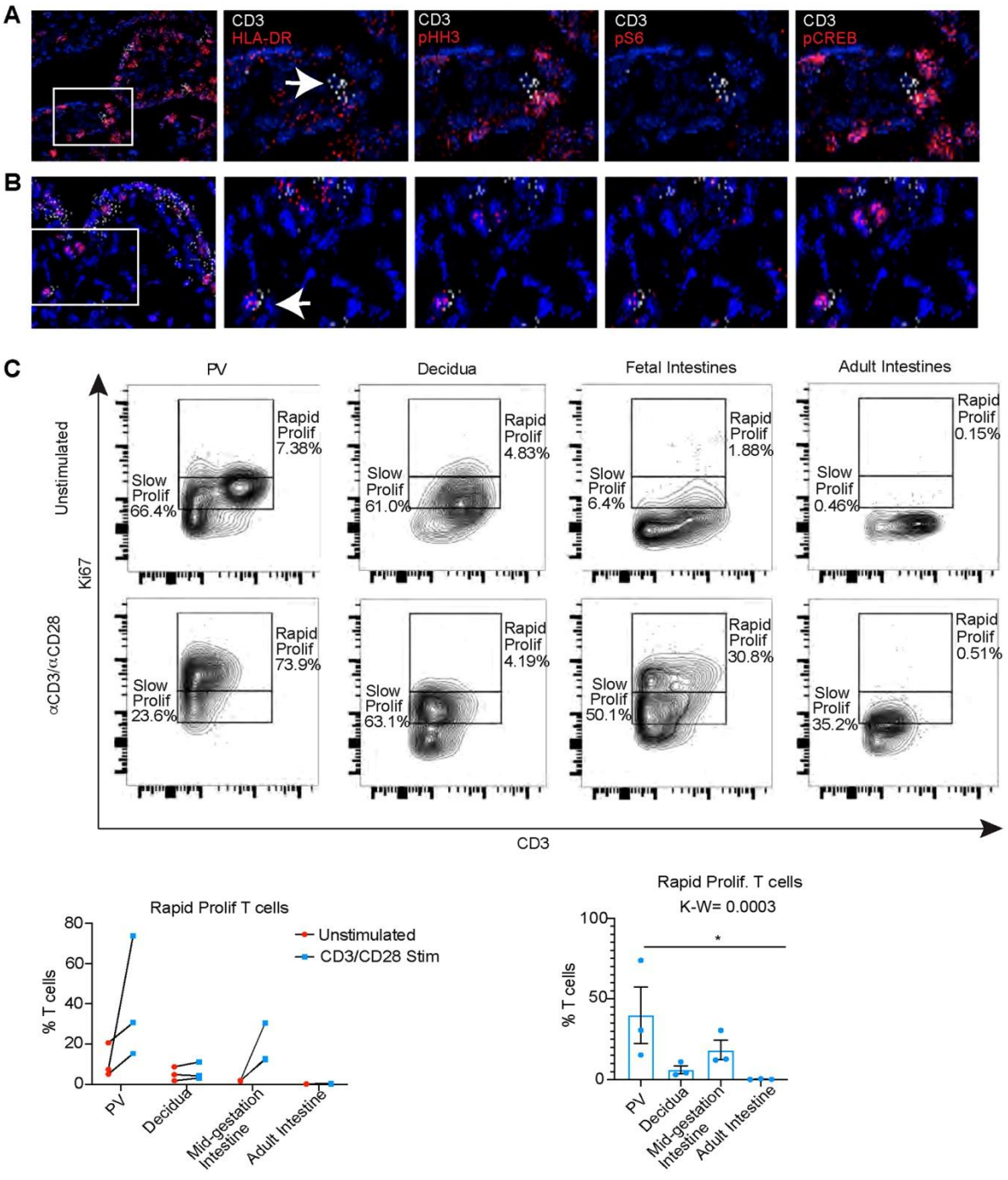

Figure 6. T cell activation in PV. (A) IMC images of inactive T cell in PV. (B) IMC images of activated T cell in PV. (C) Flow plots (top) and quantification (bottom) for proliferating ($Ki67^{hi}$) T cells after stimulation across tissues indicated. All experiments are (n=3). All graphs use mean for average values and standard error for error bars.

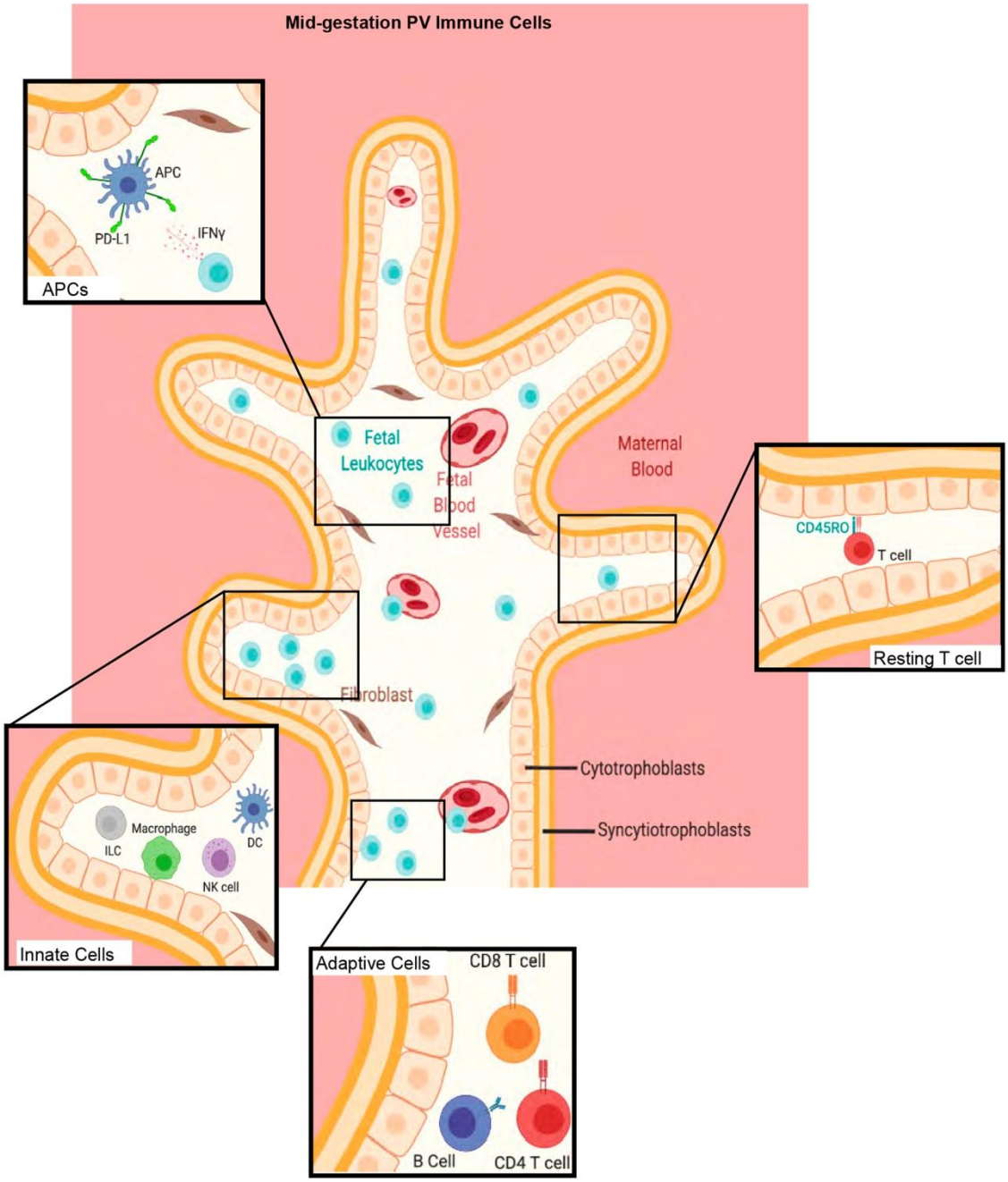

Figure 7. Summary of major findings in study. Image was generated with Biorender.com.

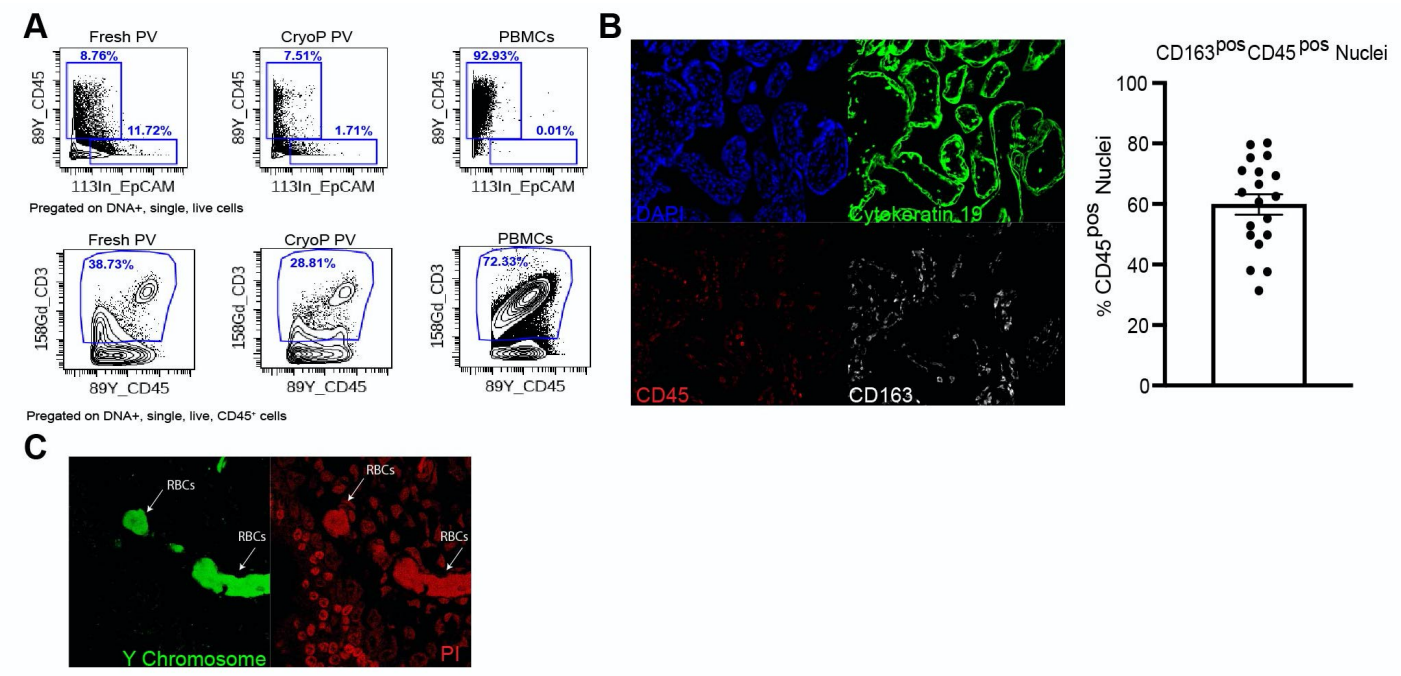

Fig. S1. (A) Comparison of CyTOF analysis of $CD45^{pos}$ and T cell abundances between fresh PV, cryopreserved PV and frozen Peripheral Blood Mononuclear Cells (PBMCs). CyTOF analysis (n=12), see Table S5 for omitted cases. (B) Splits of immunofluorescence for intravillous immune cell detection and quantification of $CD163^{hi}$ immune cells (n=19). (C) Splits for Y-chromosome *in situ* hybridization. All graphs are represented as Mean +/-SE (standard error).

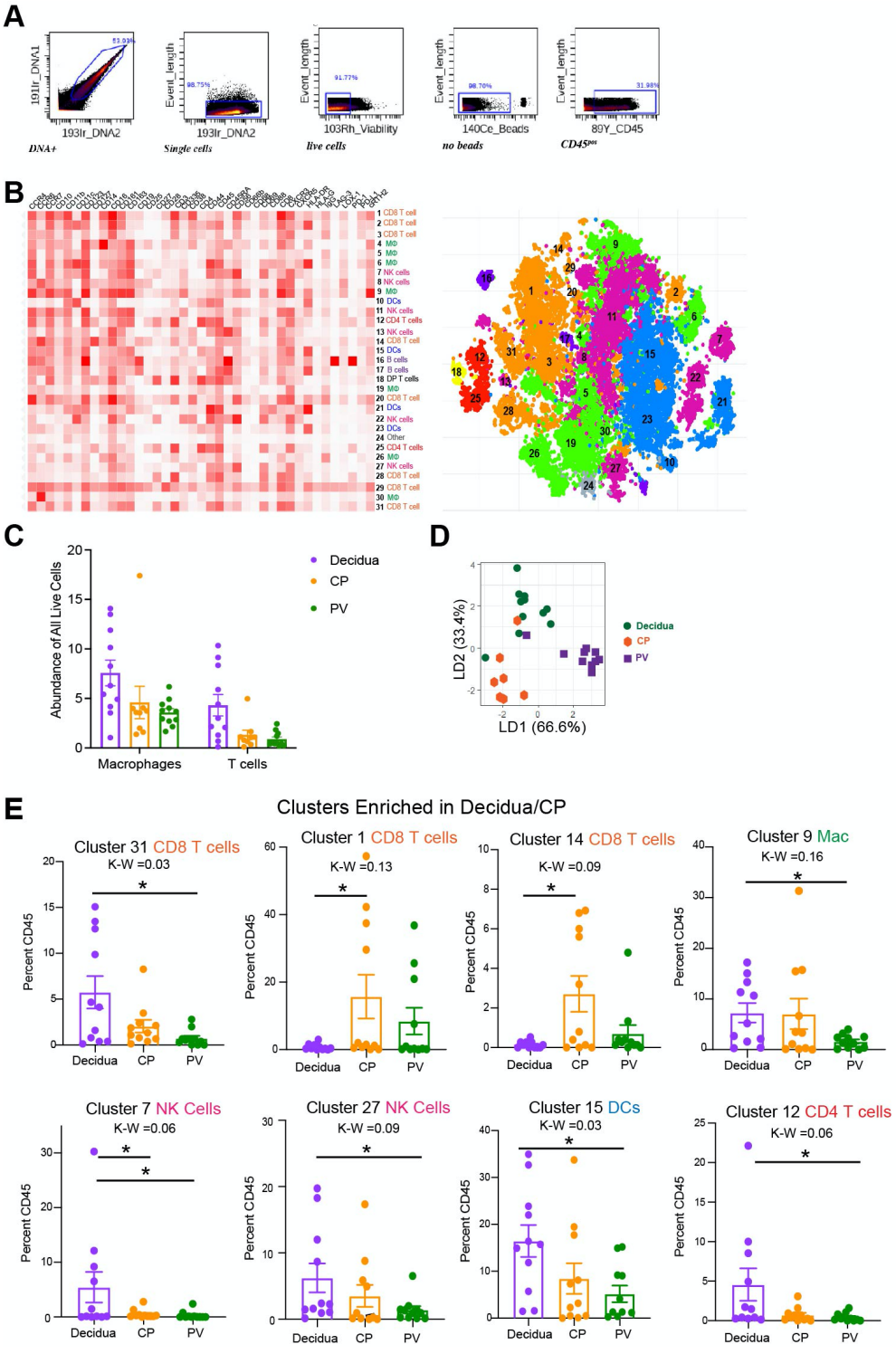

Fig. S2. (A) Pre-gating strategy for $CD45^{pos}$ population used in automated clustering. (B) Clustergrammar heatmap used for cluster identification (left) of tsne clusters mapped (right). (C) Abundance of major immune subsets as a proportion of all live cells. (D) Linkage Disequilibrium (LD) plot confirming segregation of placental layer immune profile. (E) Abundance of decidua and CP enriched clusters. CyTOF analysis starting (n=12), see Table S5 for omitted cases. * = p value < 0.05 after posthoc analysis from Kruskal-Wallis (K-W) test. All graphs are represented as Mean +/-SE (standard error).

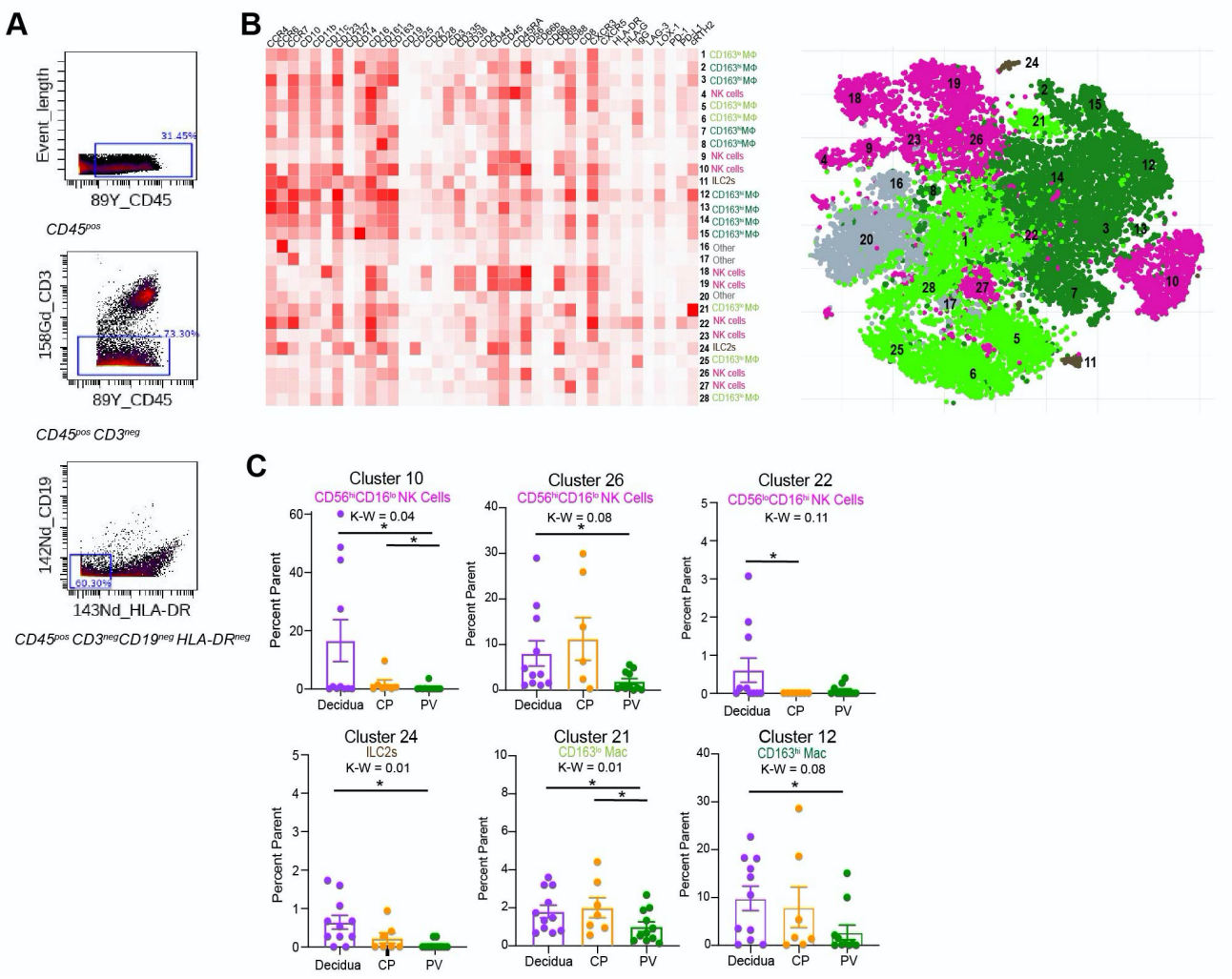

Fig. S3. (A) Pregating strategy for innate non-APC population. (B) Clustergrammar heatmap used for cluster identification (left) of tsne clusters mapped (right). (C) Cumulative data on abundance of decidua and CP enriched clusters. CyTOF analysis starting (n=12), see Table S5 for omitted cases. * = p value < 0.05 after posthoc analysis from Kruskal-Wallis (K-W) test. All graphs are represented as Mean +/-SE (standard error).

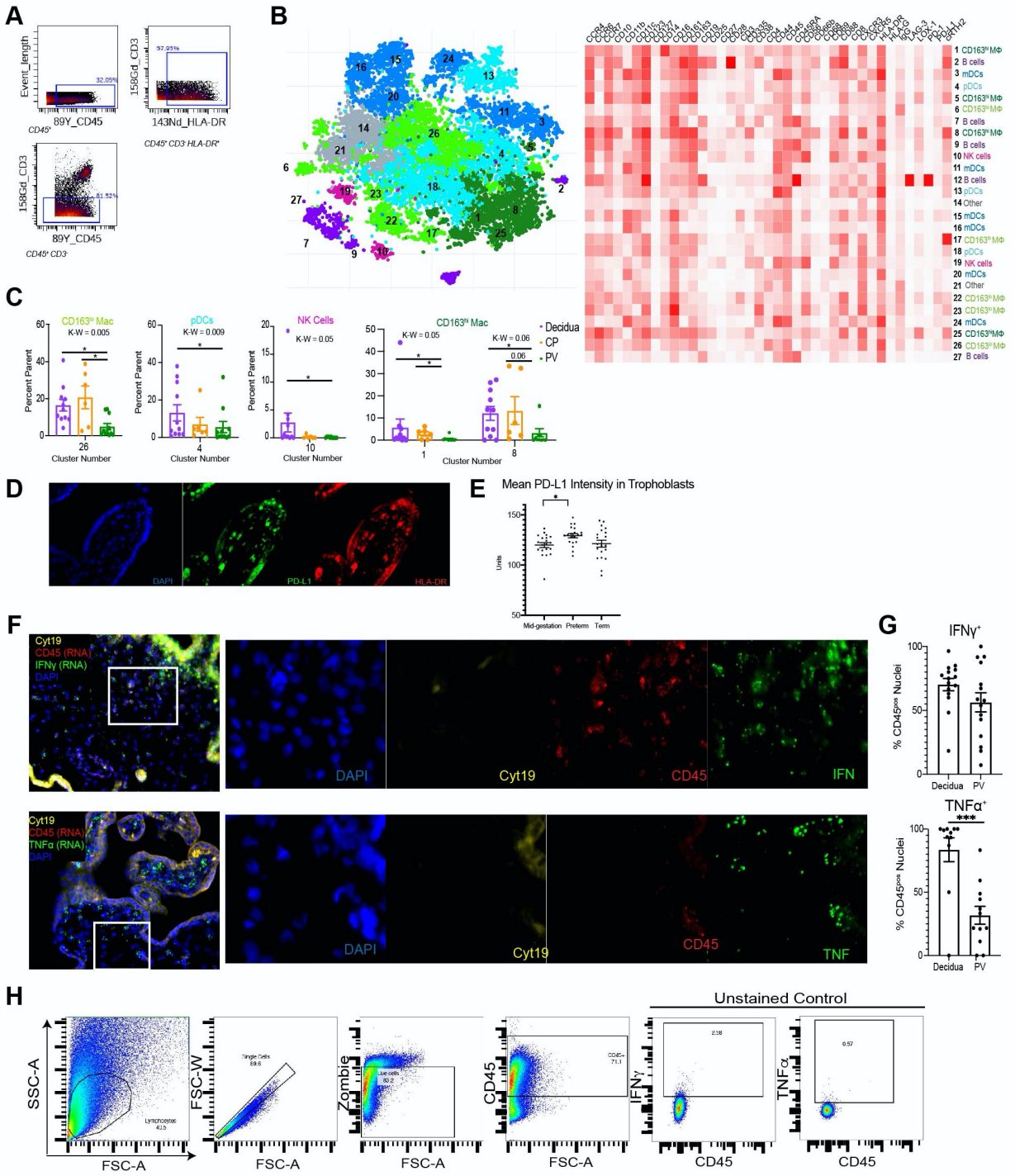

Fig. S4. (A) Pregating strategy for APC population. (B) Clustergrammar heatmap used for cluster identification (left) of tsne clusters mapped (right). (C) Cumulative data on abundance of decidua and CP enriched clusters. CyTOF analysis starting (n=12), see Table S5 for omitted cases. * = p value < 0.05 after posthoc analysis from Kruskal-Wallis (K-W) test. (D) Splits for PD-L1^{pos} PV APCs representative image. (E) Quantification of trophoblast expression of PD-L1

via IHC. (n=2) (F) Splits for dual RNA *in situ* hybridization and IF. Representative images in main figure taken from region identified in white rectangle. (G) Quantification of staining for cytokine positive immune cells in PV and decidua. (n=4) (H) Pregating for $CD45^{pos}$ population with flow cytometry. *** = p-value < 0.001 in Mann-Whitney two tailed test. All graphs are represented as Mean +/-SE (standard error).

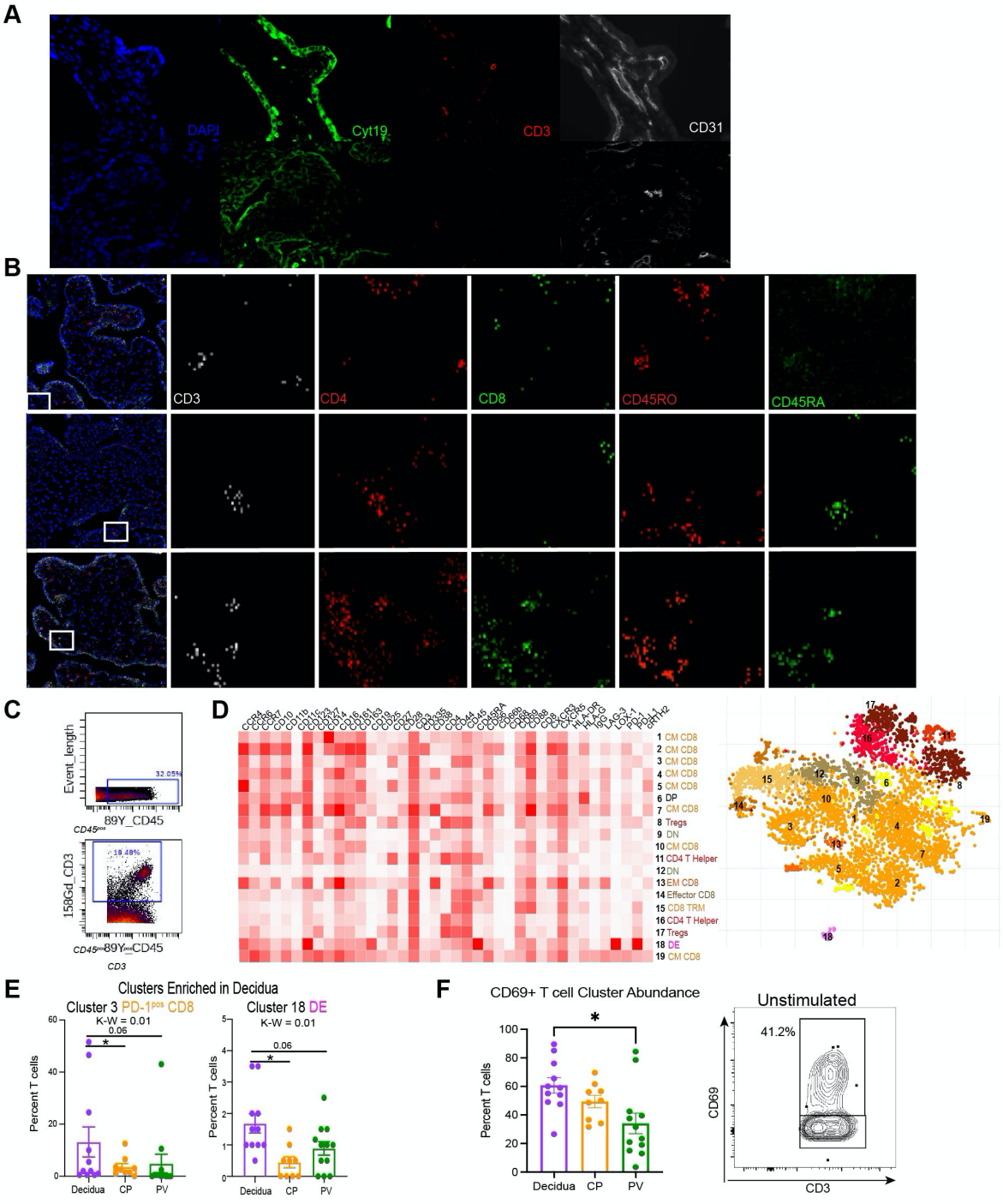

Fig. S5. (A) Splits from IF detection of T cells and PV endothelium. (B) Splits from representative IMC images of T cell subsets. T cells show in main figures identified in regions highlighted with white rectangles. (C) Pregating strategy for T cell population. (D) Clustergrammer heatmap used for cluster identification (left) of tsne clusters mapped (right). (E)

Cumulative data on abundance of decidua and CP enriched clusters. * = p value < 0.05 after posthoc analysis from Kruskal-Wallis (K-W) test. (F) Abundance of CD69+ T cells calculated by summation of all CD69+ T cell tsne clusters (left) see Table S5 for omitted cases. Representative FACS plot of $CD69^{+}$ T cells isolated from mid-gestation placenta (right). All graphs are represented as Mean +/-SE (standard error).

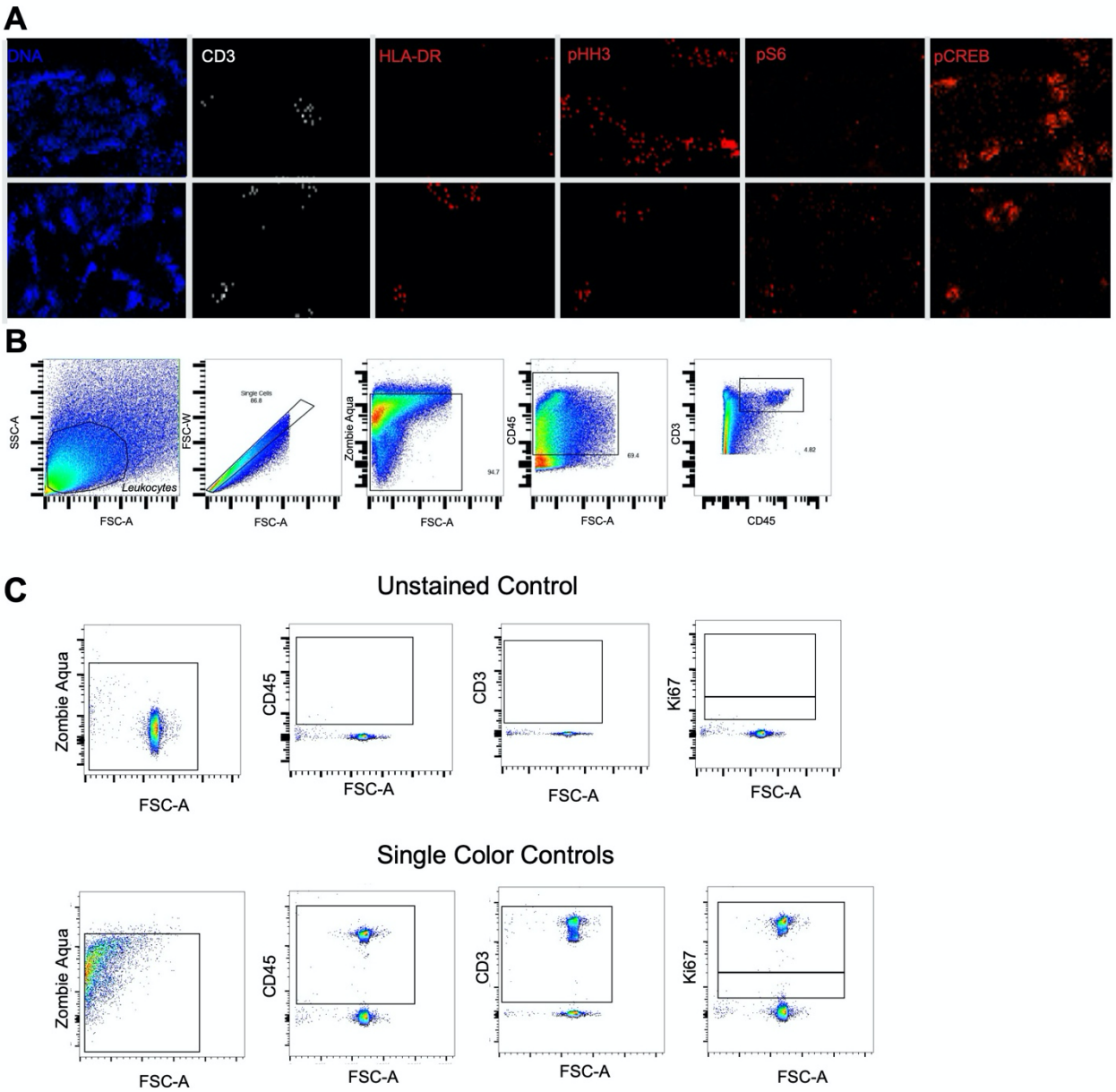

Fig. S6. (A) Splits from IMC images showing inactive and active T cells in PV. (B) Pregating strategy for CD69^{pos} and CFSE^{pos} T cells. (C) Gating for proliferative populations quantified in main text. All experiments are (n=3).

Table S1. Patient Cohort

Table S1: Patient Cohort

Demographic Information						
Sample Number	Gestational Age	Sex	Maternal Age Range	Diagnosis	Method of Delivery	Labor
1130	23 weeks	F	25-30	ET	N/A	N/A
1143	23 weeks	M	20-25	ET	N/A	N/A
1146	23 weeks	F	25-30	ET	N/A	N/A
1081	22 weeks	M	25-30	ET	N/A	N/A
1131	18 weeks	M	20-25	ET	N/A	N/A
1132	22 weeks	M	30-35	ET	N/A	N/A
1186	18-19 weeks	M	30-35	ET	N/A	N/A
1100A	21 weeks	N/A	34-40	ET	N/A	N/A
1102	21 weeks	F	40-45	ET	N/A	N/A
1055	23 weeks	F	35-40	ET	N/A	N/A
1108	22 weeks	F	25-30	ET	N/A	N/A
1038	21 weeks	M	N/A	ET	N/A	N/A
1042	22 weeks	M	N/A	ET	N/A	N/A
1094	17 weeks	F	25-30	ET	N/A	N/A
1106	21 weeks	F	30-35	ET	N/A	N/A
1165	18 weeks	M	20-25	ET	N/A	N/A
PO38	23 weeks	F	N/A	ET	N/A	N/A
1304	39 weeks	M	N/A	HT	C-section	N
1315	37 weeks	F	N/A	HT	C-section	N
1316	39 weeks	M	N/A	HT	C-section	N
1302	39 weeks	M	N/A	HT	C-section	N
1303	39 weeks	F	N/A	HT	C-section	N
1230	29 weeks	M	N/A	Hemorrage	Vaginal	Y
1236	35 weeks	M	N/A	D, HyT	C-section	N/A

Experimental Use								
RNAseq	qPCR	FISH	CyTOF	IMC	RISH	IHC	TCR Stim CFSE	TCR Stim Ki67
✓			✓		✓	✓		
✓		✓						
✓			✓					
	✓							
	✓		✓					
	✓		✓					
	✓			✓			✓	
	✓					✓		
	✓		✓					
	✓							
		✓	✓		✓			
			✓					
			✓					
			✓				✓	
			✓		✓			
			✓	✓	✓		✓	
			✓					
								✓
								✓
								✓
						✓		
						✓		
						✓		

* genetic case
ET, Elective Termination
HTD, Healthy Term
Y, Yes
N, No
D, Diabetes
Hyt, Hypertension

Table S3. Selected Immune Genes

Table S3: Selected Immune Genes

Gene Name	Expression Values								
	Decidua 1	Decidua 2	Decidua 3	CP1	CP2	CP3	PV1	PV2	PV3
PTPRC	18.25	9.53	13.57	6.64	7.22	0.21	2.84	2.84	4.34
CD3D	5.02	3.87	5.38	0	0.64	0	0	0.65	0.47
CD3G	0.63	0.3	0.67	0	0.39	0	0.12	0.12	0.21
CD3E	9.3	4.15	7.35	0.04	0.53	0	0.13	0.17	1.85
CD4	48.51	60.61	62.16	20.23	24.72	2.04	17.55	39.68	46.63
CD8A	0.38	2.85	1.73	0	0.25	0	0	0.11	0.76
IL7R	1.08	0.75	2.66	0.14	1.56	0.1	0.19	0.29	0.71
CD19	0.06	0.05	0.49	0.79	0.44	0.03	0	0.42	0.27
NCAM1	6.53	2.02	3.29	0.18	0.02	0.06	0	0.01	0.33
CD14	444.26	329.06	470.57	228.26	219.48	3.83	162.49	324.13	430.24
CD163	54.09	37.6	44.92	43.76	29.41	0.9	20.53	31.63	36.2
CD68	385.84	213.79	459.9	78.93	110.38	9.69	115.92	62.35	165.92
IL3RA	4.65	11.15	5.31	2.78	13.33	0.21	11.2	8.06	9.96
ITGAX	11.27	4.97	18.49	1.46	3.36	0.06	0.98	0.75	1.18
HLA-DRA	1,690.96	589.86	962.34	386.91	495.82	4.53	55.26	86.08	67.75
HLA-DRB5	258.75	101.54	238.74	50.52	87.15	0.99	6.51	19.9	22.32
HLA-DRB6	48.63	23.05	70.91	13.91	22.82	0.4	2.66	3.21	4.85
CD69	8.06	4.16	17.1	1.93	2.04	1.32	1.72	0.48	3.53
CD44	50.77	30.92	50.01	22.61	31.86	2	24.06	19.52	48.42
NFKB1	16.11	34.05	22.71	7.99	30.13	28.96	11.12	25.79	28.47
NFKB2	13.03	17.85	18.36	6.42	14.28	47.22	4.15	10.58	15.45
CXCL8	93.43	53.42	30.57	40.08	665	15.41	87.19	44.44	21.43
IL1B	85.82	55.8	70	4.92	60.03	0.98	4.86	3.45	15.24
IL6	2.34	5.18	3.48	5.69	14.34	22.4	16.03	6.67	12.39
IFNGR1	124.86	152.35	166.72	49.29	157.79	68.13	61.25	114.17	121.57
IFNGR2	141.04	168.79	200.74	98.05	113.48	205.37	77.54	54.45	190.82
IFNAR2	14.09	22.98	20.82	7.76	26.34	8.35	7.52	11.98	16.93
IFNAR1	26.69	33.77	34.23	14.09	29.39	29.99	12.63	17.96	32.96
TNFRSF4	4.72	4.05	10.42	2.14	7.98	0	5.1	5.42	5.79
TNFRSF14	13.04	11.26	17.46	4.76	10.05	2.69	10.73	7.98	16.69
TNFRSF1B	54.03	90.41	69.25	21.9	64.87	0.52	31.26	69.05	61.91
TNFRSF11A	2.65	3.09	1.15	3.98	2.9	0.1	2.89	2.88	1.01
TNFRSF6B	5.54	5.05	4.01	1.69	3.81	4.28	3.22	1.14	4.59

Table S4. CyTOF Panel

Table S4: CyTOF Panel

Metal	Target	Clone	Vendor
89Y	CD45	HI30	Fluidigm
113In	CD88	P12/1	BioRad
115In	CD44	IM7	BioLegend
141Pr	CD66b	G10F5	BioLegend
142Nd	CD19	HIB19	BioLegend
143Nd	HLA-DR	L243	Fluidigm
144Nd	CD69	FN50	Fluidigm
145Nd	cRTH2	BM16	BioLegend
146Nd	CD8a	RPA.T8	BioLegend
147Sm	CD10	HI10a	BioLegend
148Nd	CD28	CD28.2	BioLegend
149Sm	CD25	2A3	Fluidigm
150Nd	CD38	HIT2	BioLegend
151Eu	CD123	TUGH4	BioLegend
152Sm	CD14	M5E2	BioLegend
153Eu	CD45RA	HI100	BioLegend
154Sm	CD163	GHI/61	Fludigim
155Gd	CD27	L128	Fluidigm
156Gd	CCR4	SIDI8BEE	eBiosciences
158Gd	CD3	UCHT1	BioLegend
159Tb	CD11c	Bu15	BioLegend
160Gd	IgG	MHK49	Fluidigm
161Dy	CD16	3G8	BioLegend
162Dy	CD56	NCAM16.2	BioLegend
163Dy	CXCR3	G025H7	Fluidigm
164Dy	CD161	HP-3G10	BioLegend
165Ho	LAG3	11C3C65	Fluidigm
166Er	HLA-G	87G	BioLegend
167Er	Lox1	331212	R&D Systems
168Er	CD127	A019D5	Fludiigm
169Tm	CD11b	M1/70	BioLegend
170Er	CCR7	G043H7	BiolLegend
171Yb	CD68	Y1/82A	Fluidigm
172Yb	CD274(PD-L1)	29E.2A3	BioLegend
173Yb	CD335	9E2	BioLegend
174Yb	CD4	SK3	Fluidigm
175Lu	PD-1	EH12.2H7	Fluidigm
176Yb	IL-10	JES3-19F1	BioLegend
209Bi	CXCR5	MU5UBEE	eBiosciences

Table S5. Files Omitted from CyTOF Analyses

Table S5: Files Omitted from CyTOF Analyses

Sample Name	Figures Excluded
1102 Decidua	1,2,4,5
1165 CP	1,2,4,5
PO38 PV	1,2,4
1094 CP	2,4
1130 CP	2,4
1131 CP	2,4

Table S6. Cell Type Identification

Table S6: Cell Type Identification

Cell Type	Markers
Leukocytes/Immune Cells	CD45+
T Cells	CD45+CD3+
B Cells	CD45+CD3-CD19+
Innate Cells	CD45+CD3-CD19-
CD4 T cells	CD45+CD3+ CD4+
CD8 T cells	CD45+CD3+ CD8+
Double Positive T Cells	CD45+CD3+ CD4+ CD8+
Double Negative T Cells	CD45+CD3+ CD4- CD8-
Regulatory T cells	CD45+CD3+ CD4+ CD127lo CD25+
Macrophages	CD45+CD3-CD14+
NK Cells	CD45+CD3-CD19-CD14-CD56+
Dendritic Cells	CD45+CD3-CD19-CD14-CD56- HLA-DR+
Plasmacytoid Dendritic Cells	CD45+CD3-CD19-CD14-CD56- HLA-DR+ CD11b+
Myeloid Dendritic Cells	CD45+CD3-CD19-CD14-CD56- HLA-DR+ CD123+
Innate Lymphoid Cells	CD45+CD3-CD19- CD127+
Innate Lymphoid Cells Type 2	CD45+CD3-CD19- CD127+ cRTH2+
Dual Expressing Lymphocytes	CD45+CD3+ CD19+

Table S7. Differentially Expressed Chemokines

Table S7: Differentially Expressed Chemokines

Gene Name	Expression Values								
	Decidua 1	Decidua 2	Decidua 3	CP1	CP2	CP3	PV1	PV2	PV3
CCL20	1.8	1.82	1.54	1.86	19.35	17.19	1.92	0.6	0.82
CXCL1	13.87	30.47	10.96	10.19	63.07	200.51	10.3	54.14	6.71
CXCL2	15.56	2.21	29.92	11.11	19.91	291.33	11.76	2.57	5.55
CXCL9	8.14	6.96	6.01	2.43	0.11	0	0	0.05	0.4
CXCL10	61.44	37	50.4	17.1	4.66	0.45	4.13	1.44	18.45
CXCL11	3.71	2.37	2.43	0.37	0.31	0	0.25	0.32	2.03
CXCL13	57.5	5.58	7.54	0.08	0	0	0	0	2.3
CCR6	0.08	0.53	0.26	0.03	0	0.04	0	0	0.02
CCL19	0.67	0.65	1.41	0	0	0	0	0	0.19
CCL21	147.98	121.42	54.91	3.61	58.4	0.1	0.62	0.07	0.4
CXCL12	17.24	6.77	14.59	4.01	1.36	0.01	3.03	1.18	4
CCL17	2.51	3.02	0.67	0	0	0	0	0	0.12
CCL8	176.57	38.1	73.7	40.76	13.42	1.98	3.02	2.41	22.94
CCL5	28.58	34.01	143.58	11.25	16.63	0.12	4.67	5.99	27.3
CCL14	14.33	1.65	6.49	0.15	0.18	0	0	0.04	0.4
CCL14-15	0.17	0.41	5.36	0.91	1.52	0	0	0	0
CCL23	13.59	4.29	19.25	0	0.4	0	0.26	1.1	2.08
CCL4	173.82	72.43	292.49	51.6	61.12	3.65	28.47	17.57	77.83
CXCR3	4.35	8.74	10.61	0.06	0.11	0	0	0.14	1.68

Table S8. IMC Panel

Table S8: IMC Panel

Metal	Target	Clone	Vendor
115In	CD44	IM7	BioLegend
142Nd	CD19	6OMP31	Fluidigm
143Nd	Vimentin	D21H3	Fluidigm
144Nd	CD14	EPR3653	Fluidigm
147Sm	CD163	EDHu-1	Fluidigm
148Nd	PanKeratin	C11	Fluidigm
151Eu	CD31	EPR3094	Fluidigm
152Sm	CD45	D8M81	Fluidigm
156Gd	CD4	EPR6855	Fluidigm
160Gd	IgG	MHK49	Fluidigm
161Dy	Ki67	8D5	BioLegend
162Dy	CD8a	C8/144B	Fluidigm
164Dy	pZAP70		Cell Signaling
165Ho	pCREB	87G3	Cell Signaling
166Er	CD45RA	HI100	Fluidigm
167Er	p44/42	D13.14.4E	Cell Signaling
169Tm	pSTAT3	A1600213	Cell Signaling
170Er	CD3	polyclonal	Fluidigm
171Yb	CD66a	CD66a-B1.1	Fluidigm
173Yb	CD45RO	UCHL1	Fluidigm
174Yb	HLA-DR	LN3	Fluidigm
175Lu	pS6	D57.2.2E	Cell Signaling
176Yb	pHistoneH3	HTA28	Fluidigm

Table S9. Flow Cytometry Antibodies

Table S9: Flow Cytometry Antibodies

Fluorophore	Target	Clone	Vendor
PE-Cy7	CD3	SK7	Biolegend
PE	CD69	FN50	Biolegend
PacBlue	TNFa	Mab11	Biolegend
AF647	IFNg	4S.B3	Biolegend
Ki67	AF488		Biolegend
AF700	CD45	HI30	Biolegend